PHOTO/ELECTROCHEMISTRY & PHOTOBIOLOGY IN THE ENVIRONMENT, ENERGY AND FUEL

2006

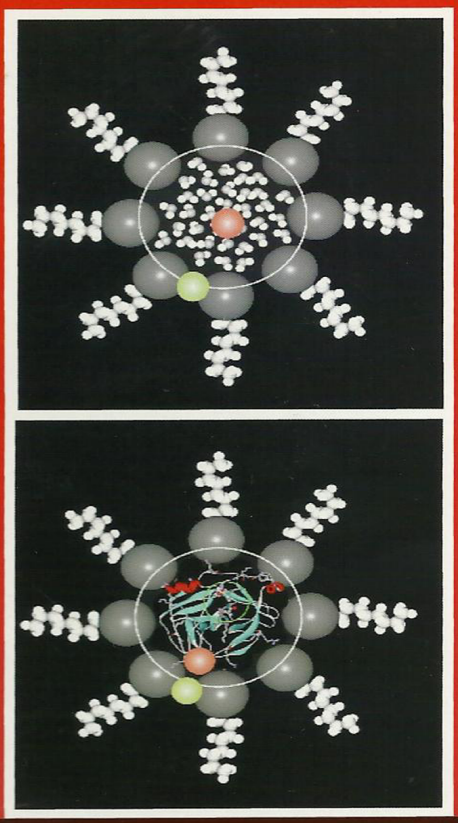

Editor-in-Chief
Satoshi Kaneco
Associate Editors
B. Viswanathan
Kunihiro Funasaka

RESEARCH SIGNPOST

Research Signpost
37/661 (2), Fort P.O., Trivandrum-695 023, Kerala, India

Photo/Electrochemistry & Photobiology in the Environment, Energy and Fuel, 2006: 103-167
ISBN: 81-308-0122-1

3 Modulation of water dynamics: A novel approach to control enzyme functionality

Rupa Sarkar and Samir Kumar Pal
Unit for Nano Science & Technology, S. N. Bose National Centre for Basic Sciences, Block JD, Sector III, Salt Lake, Kolkata 700 098, India

Abstract

Water is essential for life. Water molecules in the close vicinity of biological macromolecules, often called biological-water, are particularly important for determining biomolecular structure and function. As these waters are the part of the network of biological interfaces their ordering and dynamical behavior are significantly different than that of bulk water. In order to explore the interplay between number of water molecules and structure/function of an enzyme, selective biomolecular hydration is essential. In this review we present various restricted environments

Correspondence/Reprint request: Dr. Samir Kumar Pal, Unit for Nano Science & Technology, S. N. Bose National Centre for Basic Sciences, Block JD, Sector III, Salt Lake, Kolkata 700 098, India
E-mail: skpal@bose.res.in

(micelles, reverse micelles) with controlled degree of hydration. The environments are used as biological host of enzymes (guests). The functionality of the restricted enzymes is found to be different compared to that in bulk buffer. Our picosecond resolved fluorescence studies on the host-guest complex reveal the dynamical behavior of the enzyme and its associated solvent molecules. An attempt has been made to correlate the dynamics of the enzyme (within overall structural integrity) and its immediate environments with the functionality of the biomolecule.

1. Introduction

Dynamical freedom of biological macromolecules (protein, DNA) is found to be important for their proper function in the physiological milieu. Particularly, the immediate environments of a biomolecule impose restriction on its dynamical flexibility. For example, a significant volume of the interior of a cell is occupied by multitude of large molecules especially proteins, nucleic acids and sugars. The very high total concentration of these large molecules, called macromolecular crowding has energetic consequences that affect the functionality/recognition of a particular biomolecule controlling the net water content around the biomolecule. The water molecules in the immediate vicinity of these biomolecules (biological water) are particularly important to its structure and biological function. Rupley et al[1] showed that the dehydration of a protein, which makes it more rigid and increases its denaturation temperature, is correlated with the loss of its physiological function. In order to explore the interplay between hydration and enzymatic structure/function it is necessary to design novel experimental techniques. Modulation of the number of water molecules (hydration) available to an enzyme for modifying its activity has opened a new field of research of paramount interest[2-4]. Although several systems including protein films in various level of humidity have been developed[1], two systems have widely evolved in which the relation between water and functionality of the enzymes can be experimentally approached. One involves the entrapment of enzymes in micelle[5-7] and reverse micelle[8-10], and the other the dispersion of enzymes in nonpolar solvents[11,12]. These two nonconventional systems have a common factor: the amount of water available to enzymes can be controlled and made much lower than in the usual biological systems.

In this article, we will review our works on the control of waters around an enzyme α-chymotrypsin (CHT) by entrapment of the enzyme in nanometer sized anionic bis(2-ethylhexyl)sulfosuccinate (AOT, scheme I) reverse micelles (RM) and cationic cetyltrimethylammonium bromide (CTAB, scheme I) micelles. In our experiments we observed a retardation of enzymatic activity of CHT by more than two orders of magnitude upon encapsulation of the enzyme

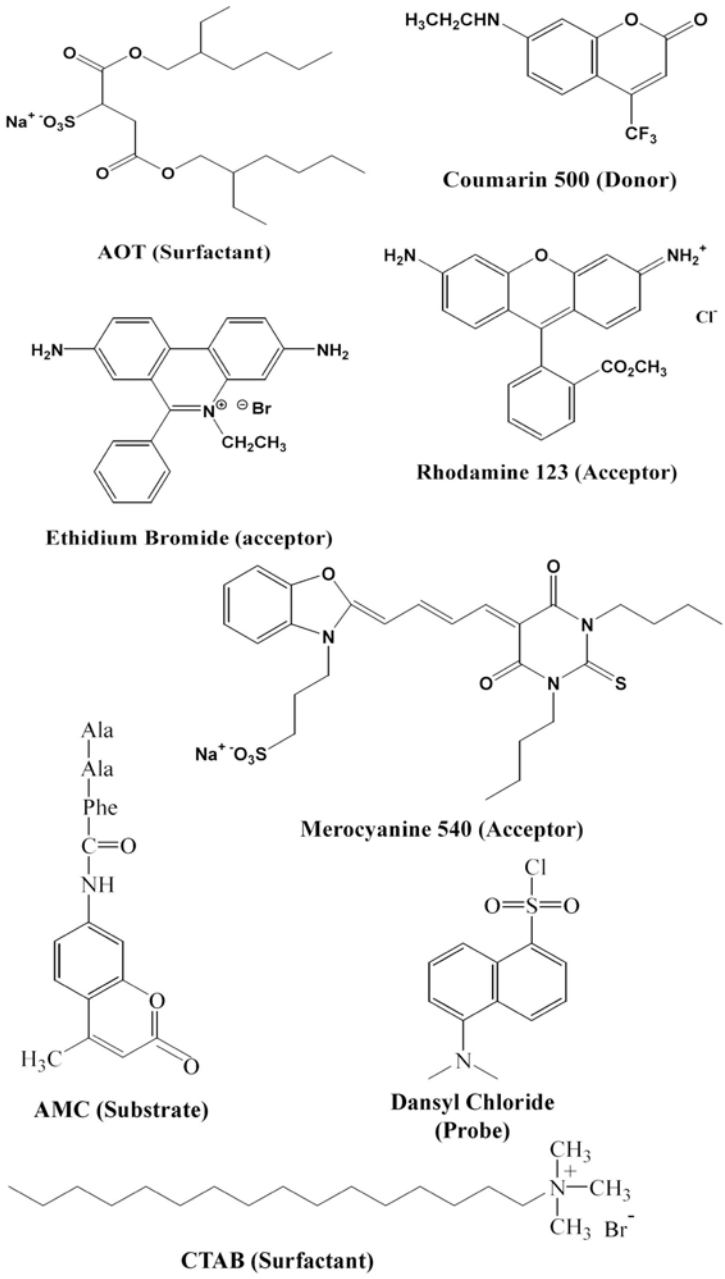

Scheme 1. Molecular structures of the anionic surfactant AOT, energy donor coumarin-500, acceptors Rhodamine 123, Ethidium Bromide, Merocyanine 540; substrate AMC, probe dansyl chloride DC and cationic surfactant CTAB.

in the reverse micelle compared to that in free buffer[4]. We propose enzyme-solvation to be one of the major factors for the retardation. In order to investigate the effect of distribution of substrate/product of the enzyme in addition to the solvation, we studied locations of substrate-mimics in the RM with and without the enzyme by using picosecond resolved Förster energy transfer (FRET) techniques[13]. Complexation of CHT with CTAB micelle

shows seven times retardation of the enzymatic activity compared to that in buffer[14]. Here we proposed slower diffusion of the substrate/product of the enzyme in the close vicinity of the micelle due to high microviscosity in the environment[14] for the retardation. Our observation of slower solvation dynamics and time resolved fluorescence anisotropy of a probe at the surface of the CTAB micelle is in agreement with the higher microviscosity around the micelle[15]. The picosecond resolved dynamical studies on the CHT-CTAB complex also reveal that a significant portion (35%) of the enzyme is involved in the complexation[14]. In this way, we examine the influence of solvation and local restriction on the reactivity of the enzyme in restricted environments, since the structures were found to be in the almost native state in these microenvironments[5,16].

2. Materials and methods

2.1. Systems

2.1.1. Micelles

In aqueous solution the amphiphilic surfactant molecules form spherical or nearly spherical aggregates called micelles, of size 1-10 nm above a certain critical concentration, known as the critical micellar concentration (CMC) and above a critical temperature, called "Kraft temperature". The size of the micellar aggregates is usually 1-10 nm and the aggregation number, i.e. the number of surfactant molecules per micelle, ranges from 20 to 200. The structure of a typical cationic micelle is schematically shown in figure 1(a). The core of a micelle is essentially "dry" and consists of the hydrocarbon chains with the polar and charged head groups projecting outward into the bulk water. The Stern layer, surrounding the core, comprises of the ionic or polar head groups, bound counter ions and water molecules. Between the Stern layer and the bulk water there is a diffuse layer, called Guoy-Chapman (GC) layer, which contains the free counter ions and water molecules. In non-ionic polyoxyethylated surfactants, the hydrocarbon core is surrounded by a palisade layer, which consists of the polyoxyethylene groups hydrogen-bonded to water molecules. Recent small angle X-ray and neutron scattering have provided detailed information on the structure of the CTAB micelles[17-19]. According to these studies; CMC and aggregation number are 0.8 and 52 respectively, the thickness of the Stern layer is 6-9 Å for CTAB micelle[18-21]. The overall radius of CTAB micelle is about 50 Å.

2.1.2. Reverse micelles

Reverse micelles are tiny aqueous droplets (Figure 1 (b)), surrounded and stabilized by a monolayer of surfactant molecules, and dispersed in a water immiscible organic solvent [for reviews see references[22,23]]. In some cases it is

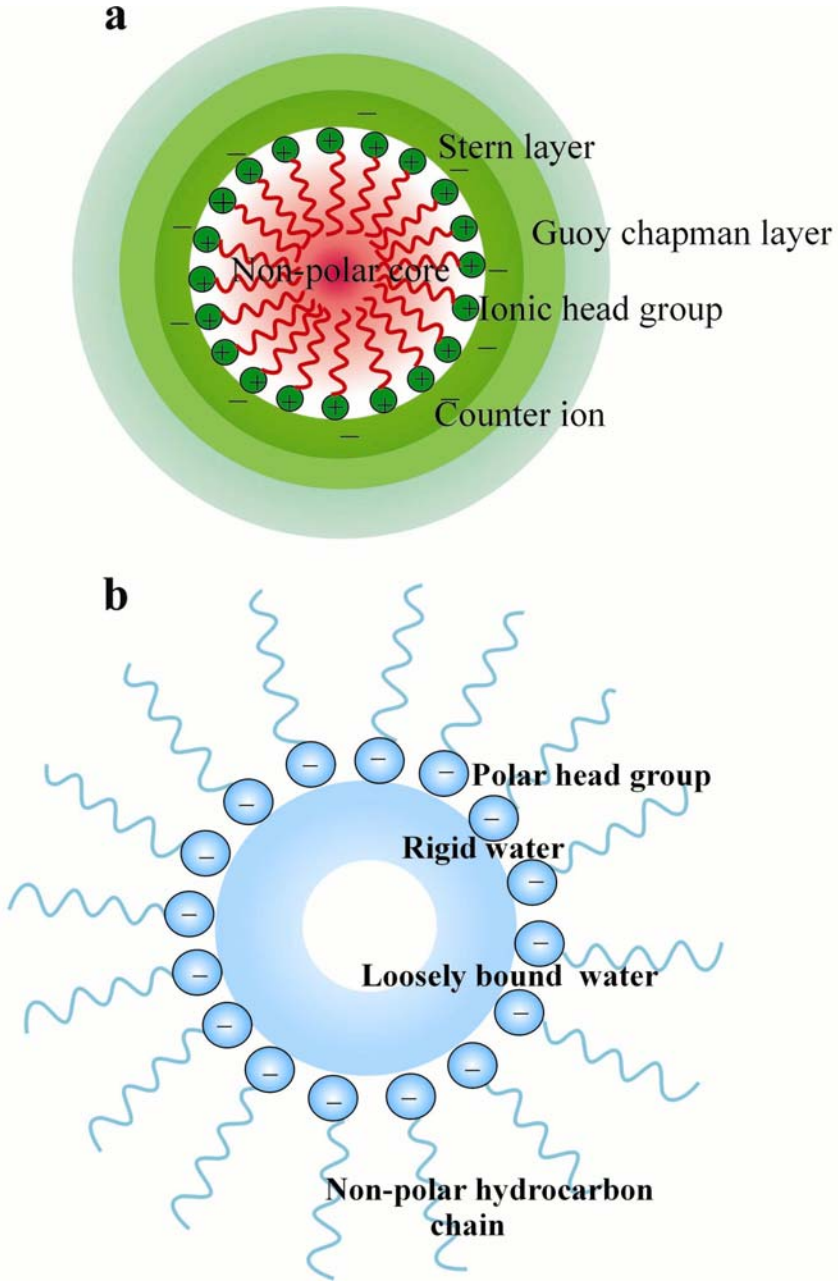

Figure 1. Schematic representation of the structure of (a) micelle (b) reverse micelle.

possible to solubilize enzymes in RM without the loss of the native structure of those enzymes. Enzymes in micellar systems usually exhibit maximal activity when the size of the internal cavity of the RM corresponds to or is close to the size of the solubilized proteins[16,24,25]. A direct relationship exists between the radius of RM of AOT (aerosol OT) and their hydration degree (w_0), which is described by the following empirical equation [23]

$$r_m(Å) \approx 2 \times w_0 \quad (1)$$

where, r_m=radius of the water pool in Å and w_0=[water]/[AOT]. For proteins with nearly spherical shape, the empirical relationship between the hydration degree of RM and molecular mass (M) of a solubilized protein is described by the following relation[25].

$$w_0 = (0.083 \pm 0.008)\sqrt{M} \quad (2)$$

2.2. Sample preparation

The lyophilized protein α-chymotrypsin (CHT) from bovine pancreas and the substrate Ala-Ala-Phe-7-amido-4-methyl-coumarin (AMC) were purchased from Sigma, DC from Molecular Probes and CTAB from Fluka. Isooctane (Spectrochem, 99.5%), bis (2-ethylhexyl) sulfosuccinate sodium salt (AOT; Fluka 99%), Coumarin 500 (C500, Exciton, 99.9%), Rhodamine 123 (Sigma, 99%), Ethidium Bromide (Molecular Probes, 99.9%) and Merocyanine 540 (Fluka, 99%) were used as received. All the aqueous solutions used in this study were prepared in phosphate buffer (0.1 M, pH 7). Chemical structures of the probes are shown in scheme I.

Inclusion of CHT in the RM was made either by adding CHT powder to the RM (at different w_0) stirring vigorously for 3 hours and filtering the solution or by injecting measured amount of aqueous CHT in the AOT-isooctane solution. Concentration of the enzyme CHT samples in the aqueous solutions was determined using the supplied (by the vendor) extinction coefficient value at 280 nm, ε_{280} (1%)=20.4 cm^{-1}. The final AOT concentration was 0.01 M-0.1 M. In most of our experiments the hydration level of the reverse micelle was maintained at w_0=10. The concentration of the RM at our [AOT] was determined on taking the aggregation constant of AOT in isooctane to be 100[22].

In order to study the interaction of CHT with CTAB micelles, we labeled the probe dansyl (DC) nonspecifically at the surface of the protein. The covalent attachment of DC to CHT (adduct formation) was achieved following the procedure from Molecular Probes[26]. Briefly, DC was first dissolved in a small amount of dimethyl formamide and then injected into the sodium bicarbonate solution (0.1 M) of CHT (pH 8.3). The reaction was terminated by adding a small amount of freshly prepared hydroxylamine (1.5 M, pH 8.5) after incubating it for 1 h at 4-8 ^oC with continuous stirring. The solution was then dialyzed exhaustively against phosphate buffer (0.1M) to separate adducts (DC-CHT) from any unreacted DC and its hydrolysis product. It should be noted that DC-CHT complexes (CHT:DC=1.7:1) are quantitatively formed because of covalent synthesis. The enzyme concentration is maintained higher than that of the probe DC in order to avoid spatial heterogeneity in the location of the probe DC. The DC labeled CHT-micelle complexes were prepared by mixing of

CTAB (50 mM) with DC tagged CHT (250 μM) in a neutral buffer solution. Sample preparation techniques were detailed in the original publications.

2.3. Methodology

2.3.1. Instrumental setup

Steady-state absorption and emission were measured with Shimadzu Model UV-2450 spectrophotometer and Jobin Yvon Model Fluoromax-3 fluorimeter respectively. Schematic ray diagrams of these two instruments are shown in figure 2 and 3 respectively. All transients were taken by using picosecond-resolved time correlated single photon counting (TCSPC) technique. The schematic block diagram of a TCSPC system is shown in figure 4. Details of the TCSPC systems including instrument response function (IRF)

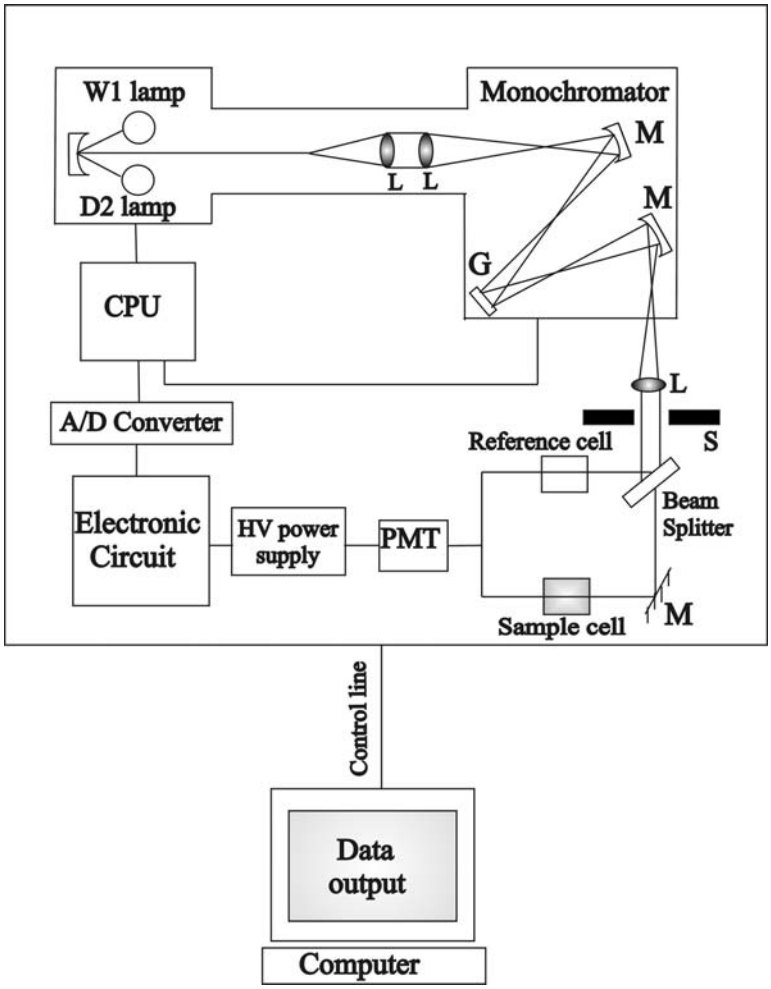

Figure 2. Schematic ray diagram of an absorption spectrophotometer. Tungsten halogen (W1) and Deuterium lamps (D2) are used as light sources in the visible and UV regions respectively. M, G, L, S, PMT indicate mirror, grating, lens, shutter and photomultiplier tube respectively.

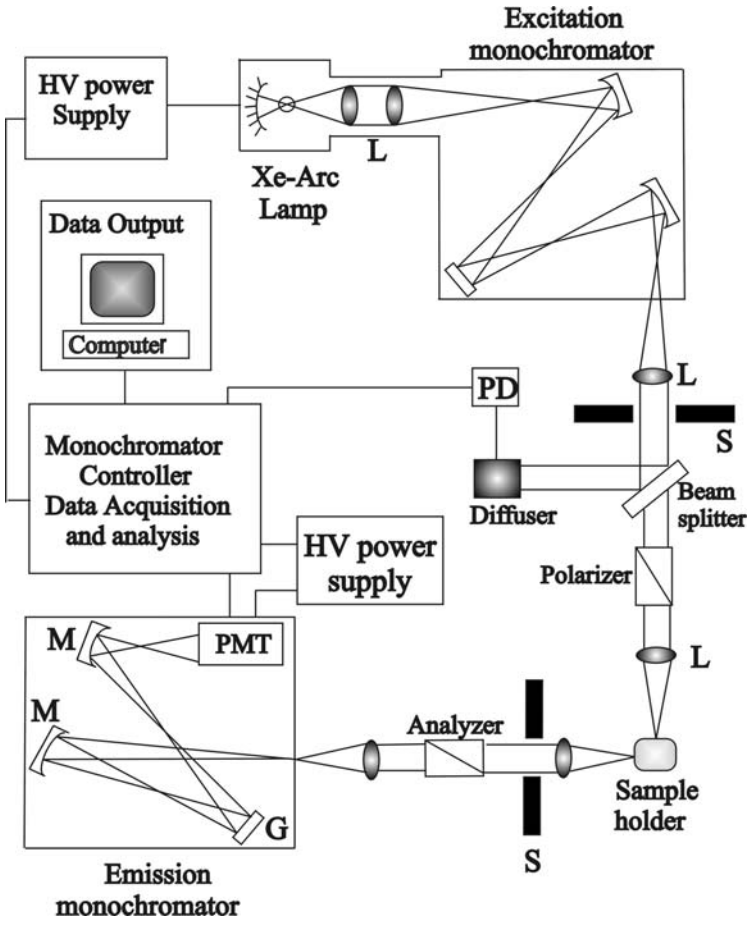

Figure 3. Schematic ray diagram of an emission spectrofluorimeter. M, G, L, S, PMT and PD represent mirror, grating, lens, shutter, photomultiplier tube and reference photodiode respectively.

and excitation wavelengths used in our experiments are given in the original publications. Liquid scatterers were used to measure the full width at half maximum (FWHM) of the instrument response functions (IRF). The fluorescence from the sample was detected by a photomultiplier after dispersion through a grating monochromator. For all transients the polarizer in the emission side was adjusted to be at 54.7° (magic angle) with respect to the polarization axis of excitation beam.

2.3.2. Enzyme kinetics

In order to measure enzymatic activity of CHT in various environments, we follow a mechanism originally proposed by Michaelis and Menten[27]. According to this mechanism a simple enzymatic reaction might be written as

$$E + S \underset{k_{-1}}{\overset{k_1}{\rightleftharpoons}} ES \xrightarrow{k_2} E+P \qquad (3)$$

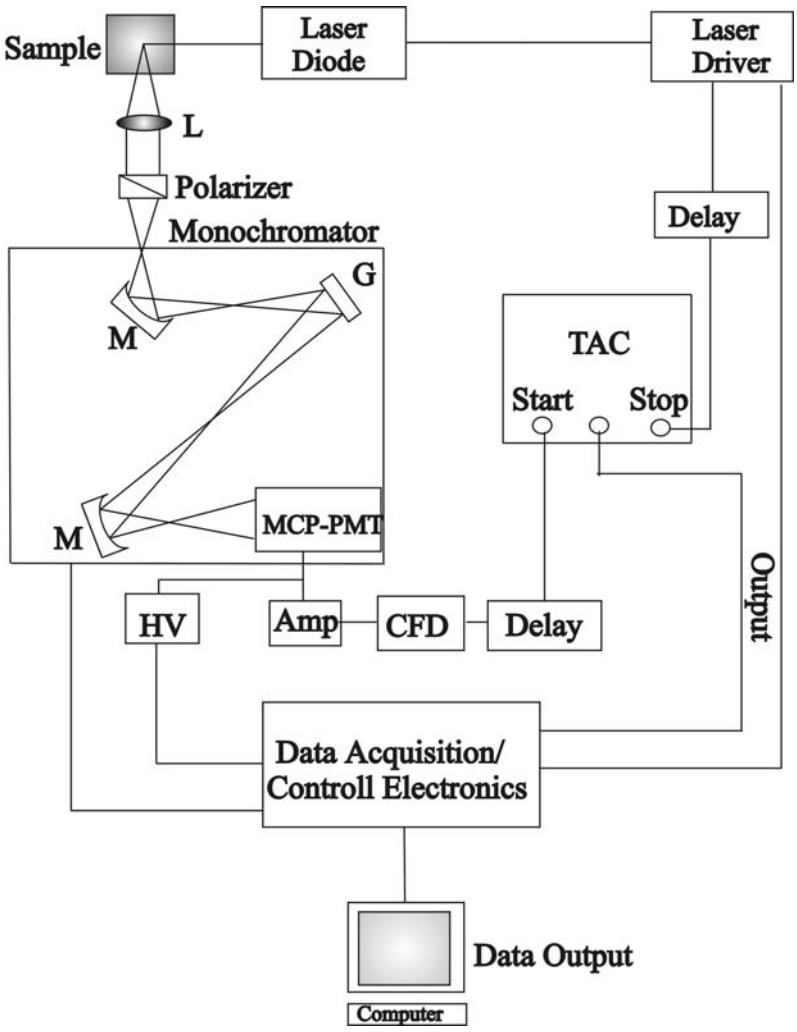

Figure 4. Schematic ray diagram of a time resolved single photon counting spectrometer. A signal from microchannel plate photomultiplier tube (MCP-PMT) is amplified (Amp) and connected to start channel of time to amplitude converter (TAC) via constant fraction discriminator (CFD) and delay. The stop channel of the TAC is connected to the laser driver via a delay line. L, M, G and HV represent lens, mirror, grating and high voltage source respectively.

where E, S and P represent the enzyme, substrate and product. ES is the transient complex of the enzyme with the substrate. The scheme assumes the following facts:

i) Enzyme first combines with substrate to form enzyme-substrate complex in a relatively fast reversible step.
ii) The ES complex then breaks down in a slower second step to yield free enzyme and reaction product P.

As the breakdown of ES to product is the slowest step, rate of reaction,

$v_0 = k_2 [ES]$ (4)

Total enzyme concentration at any instant $[E_t]$ = sum of free and substrate bound enzyme.
Free enzyme at any instant is $([E_t] - [ES])$
Rate of formation of ES = $k_1[E] [S] = k_1\{[E_t]-[ES]\} [S]$
Rate of breakdown of ES = $(k_{-1} + k_2) [ES]$
Applying Steady State concept,

$$k_1 \{[E_t] – [ES] \} [S] = (k_{-1} +k_2) [ES] \quad (5)$$

or $k_1 [E_t] [S] – k_1 [ES] [S] = k_{-1} [ES] + k_2 [ES]$
or $k_1 [E_t] [S] = \{k_1 [S] + (k_{-1} + k_1) \} [ES]$
or $[ES] = k_1 [E_t] [S] / \{ k_{-1} +k_2 + k_1 [S]\}$
or $[ES] = [E_t] [S]/ \{(k_{-1}+k_2)/k_1 +[S]\}$
or $[ES] = [E_t][S]/ (K_m + [S])$ (6)

K_m is called Michaelis constant, $K_m = (k_{-1} + k_2)/ k_1$ (7)

Now, $v_0 = k_2 [ES] = k_2 ([E_t] [S]/(K_m + [S]))$.
At high [S], $[S] >> K_m$, $v_0 = v_{max}$
$\therefore v_0 = v_{max} = k_2 [E_t][S]/[S] = k_2[E_t]$
Therefore, $v_0 = v_{max} [S] /(K_m + [S])$ (8)

This equation is known as Michaelis-Menten equation. It is the rate equation for one-substrate catalyzed reaction. If we take the reciprocal of both sides of Michaelis-Menten equation we get

$1/v_0 = (K_m + [S])/ v_{max} [S]$
$1/v_0 = K_m/ v_{max} [S] + 1/ v_{max}$ (9)

This form of Michaelis-Menten Equation is known as Lineweaver-Burk equation. For enzymes obeying Michaelis-Menten Equation, a plot of $1/v_0$ vs $1/[S]$ would be a straight line.

The quantity v_{max} varies greatly from enzyme to enzyme. For two steps enzyme reaction, $v_{max}=k_2[E_t]$ where k_2 is the rate limiting. If for three steps mechanism k_3 is rate limiting, then $v_{max}=k_3 [E_t]$. Therefore it is more general to designate rate constant of rate limiting step as k_{cat}. For two steps, $k_2= k_{cat}$, for three steps $k_3 = k_{cat}$. Therefore, Michaelis-Menten equation becomes

$$v_0=v_{max}[S] / (K_m + [S]) = k_{cat}[E_t][S]/ (K_m + [S]) \quad (10)$$

k_{cat} is a first order rate constant and has units of reciprocal time.

To compare catalytic efficiencies of enzymes the ratios k_{cat}/K_m of different enzymes is to be compared. It is called specificity constant, which is the rate constant for the conversion of (E + S) to (E + P). When $[S]<<K_m$,

$$v_0 = k_{cat} / K_m .[E_t] [S] \quad (11)$$

v_0 depends on $[E_t]$ and [S]. k_{cat}=second order rate constant. Therefore the unit of k_{cat} / K_m is $M^{-1}s^{-1}$.

2.3.3. Förster resonance energy transfer (FRET)

In order to estimate fluorescence resonance energy transfer efficiency of the donor (C500) and hence to determine distances of donor-acceptor pairs, we followed the methodology described in the chapter 13 of reference [28]. The Förster distance (R_0) is given by,

$$R_0 = 0.211 [\kappa^2 n^{-4} Q_D J(\lambda)]^{1/6} \text{ (in Å)} \quad (12)$$

Where κ^2 is a factor describing the relative orientation in space of the transition dipoles of the donor and acceptor. For donor and acceptors that randomize by rotational diffusion prior to energy transfer, the magnitude of κ^2 is assumed to be 2/3. In the present study the same assumption has been made, and it has further been justified by time-resolved anisotropy measurements of the donor and acceptor molecules (see below). The refractive index (n) of the medium is assumed to be 1.4. Q_D, the quantum yield of the donor in the absence of acceptor is measured to be 0.46 and 0.48 respectively in the RM without and with the enzyme CHT. $J(\lambda)$, the overlap integral, which expresses the degree of spectral overlap between the donor emission and the acceptor absorption is given by,

$$J(\lambda) = \frac{\int_0^\infty F_D(\lambda)\varepsilon_A(\lambda)\lambda^4 d\lambda}{\int_0^\infty F_D(\lambda) d\lambda} \quad (13)$$

Where $F_D(\lambda)$ is the fluorescence intensity of the donor in the wavelength range of λ to $\lambda+d\lambda$ and is dimensionless. $\varepsilon_A(\lambda)$ is the extinction coefficient (in $M^{-1}cm^{-1}$) of the acceptor at λ. If λ is in nm, then $J(\lambda)$ is in units of $M^{-1}cm^{-1}nm^4$.

Once the value of R_0 is known, the donor-acceptor distance (r) can be easily calculated using the formula,

$$r^6=[R_0^6(1-E)]/E \quad (14)$$

Here E is the efficiency of energy transfer. The transfer efficiency is measured using the relative fluorescence intensity of the donor, in absence (F_D) and presence (F_{DA}) of the acceptor. The efficiency E is also calculated from the lifetimes under these respective conditions (τ_D and τ_{DA}):

$$E=1-(F_{DA}/F_D) \quad (15a)$$

$$E=1-(\tau_{DA}/\tau_D) \quad (15b)$$

The distances measured by using equations 15a and 15b are revealed as R^S (steady state measurement) and R^{TR} (time resolved measurement) respectively.

2.3.4. Solvation and rotational relaxation dynamics

For every sample solution, the fluorescence transients were measured as a function of detection wavelength. The observed fluorescence transients were fitted by using a nonlinear least squares fitting procedure (software SCIENTIST) to a function comprising of the convolution of the instrument response function with a sum of exponentials. The purpose of this fitting is to obtain the decays in an analytic form suitable for further data analysis. For each detection wavelength, the transient was normalized by using the steady-state spectrum. To construct time-resolved emission spectra after the excitation pulse, we adopted the method of the reference [29].The resulting time-resolved emission spectra (TRES) were fitted with a Lognormal shape function to estimate the spectrum maximum $\nu(t)$. The temporal Stokes shift can be represented by the time dependence of the fit. By following the time-resolved emission, we constructed the solvation correlation function, $C(t) = [\nu(t)-\nu(\infty)]/[\nu(0)-\nu(\infty)]$, where $\nu(0)$, $\nu(t)$ and $\nu(\infty)$, denote the observed emission energies (in wavenumbers) at time 0, t and ∞, respectively. For time resolved area normalized emission spectral (TRANES) analysis, we adopted methods as described in the references[30-32], which is a model free modified version of TRES mentioned above. A useful feature of the method is that an isoemissive point in the spectra involves two emitting species, which are kinetically coupled either irreversibly or reversibly or not coupled at all.

For anisotropy measurements emission polarization was adjusted to be parallel or perpendicular to that of the excitation and define anisotropy as $r(t)=[I_{para}-G\cdot I_{perp}]/[I_{para}+2\cdot G\cdot I_{perp}]$. I_{para} and I_{perp} are detected emission intensities with polarization parallel and perpendicular respectively with respect to the excitation laser pulse. The magnitude of G, the grating factor of the emission monochromator of the TCSPC system was measured by using a coumarin dye in methanol and following longtime tail matching technique[33]. The steady-state anisotropy (r) was measured by using the automatic option of the fluorimeter.

3. α−chymotrypsin in reverse micelle

3.1. Structure of α−chymotrypsin inside reverse micelle

Figure 5 upper depicts high resolution X-ray structure of the enzyme CHT[34]. The enzyme, isolated from bovine pancreas belongs to a class of digestive serine protease, and has biological function of hydrolyzing polypeptide chains. It is a globular protein with molecular weight of 24,800 DA and dimensions 40×40×51 Å[16]. It can therefore be represented as a sphere with a radius of approximately 22 Å[3]. Lower panel of figure 5 shows the Circular Dichroism (CD) spectra of

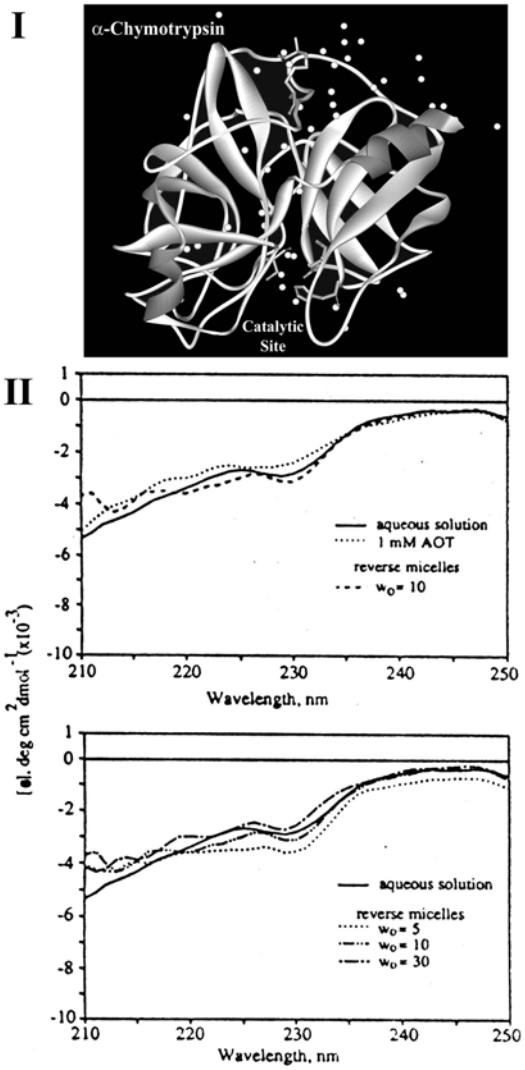

Figure 5. *(I)*. A schematic structure of the enzyme α-chymotrypsin. The enzyme structure was downloaded from the protein data bank (ID code 2CHA) and handled with program WEBLAB VIEWERLITE. *(II)*. CD spectra of α-chymotrypsin in aqueous and AOT-isooctane reverse-micelle solutions. [θ] = Mean residual ellipticity. Reprinted with permission from reference[16]. Copyright 1993 Elsevier.

CHT in buffer (native form) and in reverse micelle[16]. Both the CD spectra are indicative of little change in secondary structure upon incorporation of the protein inside reverse micelle of w_0=10 from the native protein. Structural change of the protein for other w_0 values is also shown for comparison. As evidenced in the reference [16] for lower w_0 values (w_0=5) a small increase in helical content is shown which might be the consequence of absence of free water molecules. Because all the water molecules are in strong binding interaction with the polar head groups of surfactant molecules. Higher active-enzyme concentration is reported for higher w_0 values[16]. The structural integrity of CHT in the RM was also confirmed by EPR and active site titration studies ([16] and references therein).

3.2. Enzymatic activity in the nanospace of reverse micelle

The role of protein hydration in enzyme function (catalysis) is well recognized and has recently been reviewed by several authors[1,35-37]. As mentioned above reverse micelle (RM) is a system that is commonly used to control the degree of hydration. Equations 1 and 2 then indicate that the maximum degree of hydration for this protein is expected[16,24,25] to occur at $w_0 \approx$ 10-12, where the radius of the water pool of the RM is of the same order as that of the CHT. Recently, Zewail's group found a correlation between the ultrafast surface hydration and the functionality of the enzyme CHT[38]. Fluorescence up-conversion technique with femtosecond time-resolution indicate that in the physiological active state of the enzyme, water molecules at the surface possess relatively a high degree of mobility, whereas in the inactive state the water is more rigidly structured.

Here, by using Michaelis-Menten kinetics we obtained the equilibrium and rate constants for the enzymatic activity in buffer at pH=7.0. Then we measured the catalytic rates of CHT in RM with various degrees of hydration (w_0) and compared them with those observed in the bulk buffer (physiological condition). We followed this procedure to examine the influence of degree of hydration on reactivity in the aqueous and confined (RM) environments. Note here that the reactions were studied at those values of w_0 where the native structure of CHT was preserved. Circular dichroism (CD), electron paramagnetic resonance (EPR) and active-site titration studies ([16] and references therein) made previously have indicated that encapsulation of CHT with $w_0 > 10$ brings out negligible changes in the global structure of the protein. Interestingly, the perturbation is also negligible even when w_0=10[16]. We are therefore studying the enzymatic reaction in the limit of the overall structural integrity of CHT.

Enzymatic activity. Activity measurements were performed using Ala-Ala-Phe-7-amido-4-methyl-coumarin (AMC) as the substrate. Concentration

of the substrate in aqueous buffer was estimated on taking extinction coefficient value at 325 nm to be 15.9 $mM^{-1}cm^{-1}$. The enzyme cleaves the substrate and produces a free coumarin derivative. The absorbance of this product (coumarin derivative) was monitored in absorption spectrophotometer. A cell of 1cm path length was used for measurements both in aqueous buffer (pH 7.0) and RM. Enzyme-substrate reactions in the aqueous buffer were started by the addition of an aliquot (20 μL) of the stock aqueous buffered enzyme solution to the pre-equilibrated desired AMC buffer solution at 25°C. The final enzyme concentration was 0.668 μM. The initial concentration of AMC was maintained in excess to that of the enzyme and was varied over a wide range. The increase in absorption at 370 nm due to the release of 7-amido-4-methyl-coumarin (ε_{370} = 7.9 mM^{-1} cm^{-1}) was followed (Figure 6) as time progresses. Note here that the substrate does not absorb at this monitoring

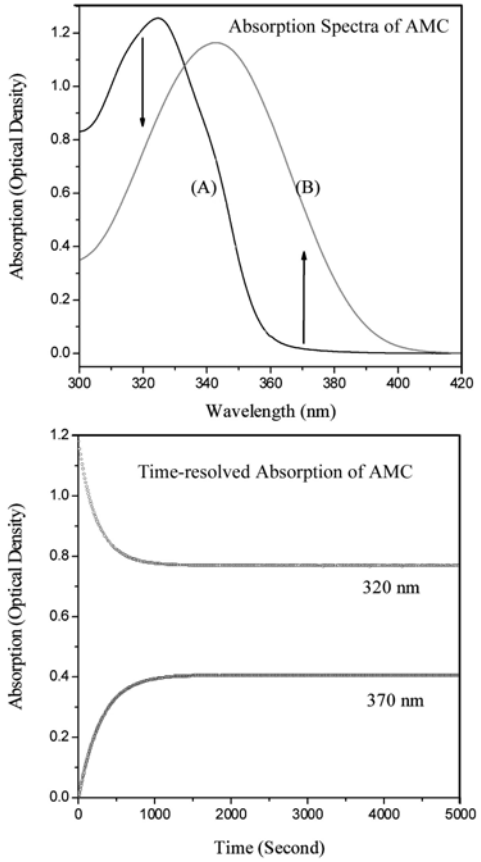

Figure 6. *Upper*. Absorption spectra of the substrate (A) and the released coumarin derivative product (B). Arrows indicate the wavelengths (320 nm and 370 nm), which were used to monitor the time-resolved absorbances as shown in the lower panel. *Lower*. The absobances at 320 nm (top) and 370 nm (bottom) as a function of time. Decay in the short wavelength (320 nm) and rise in the long wavelength (370 nm) indicate a spectral shift due to catalytic activity on the substrate.

wavelength. Initial rates were measured in the regime where the absorbance varies *linearly* with time. The reaction followed the Michaelis-Menten kinetics[39]. The apparent K_m and k_{cat} values were derived by least squares fitting of the double reciprocal Lineweaver-Burk plot (Figure 7).

To measure the rates of enzyme-substrate reactions in RM at various w_0, the stock substrate was first injected into the AOT solution and stirred until the solution became clear. Subsequently, the stock enzyme solution (10 μL) was added to the AOT solution. The cuvette was inverted several times and the absorbance was measured for 1 hour at 370 nm. The final enzyme and substrate

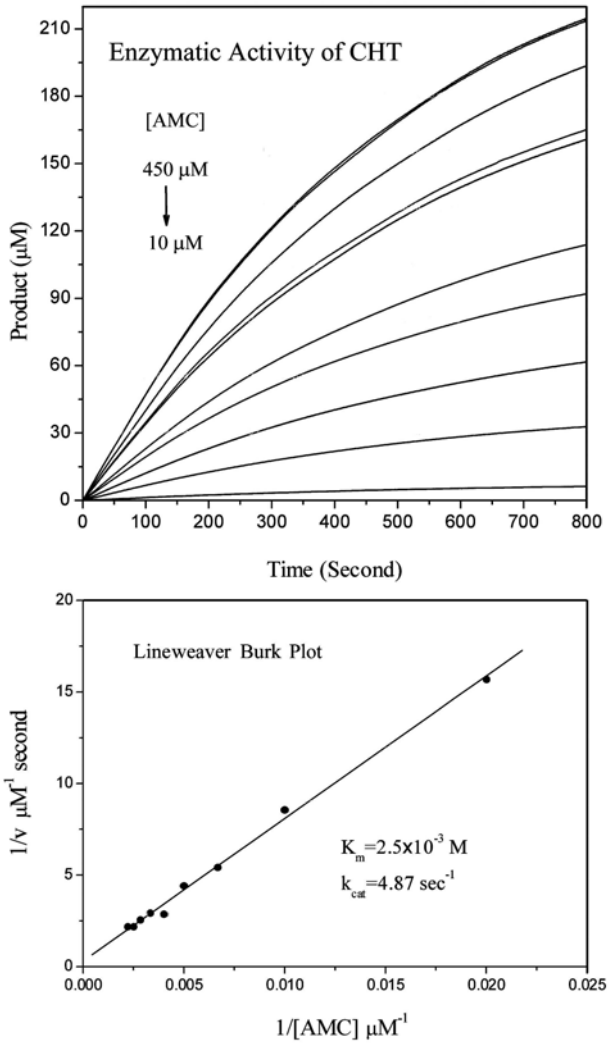

Figure 7. *Upper*. The concentrations of the product as a function of time at various substrate concentration. The enzyme concentration was kept constant at 668 nM. *Lower*. Lineweaver-Burk plot of the enzyme CHT showing its catalytic activity with substrate AMC in aqueous buffer pH = 7.0. The solid line is a linear fit following Michaelis-Menten kinetics.

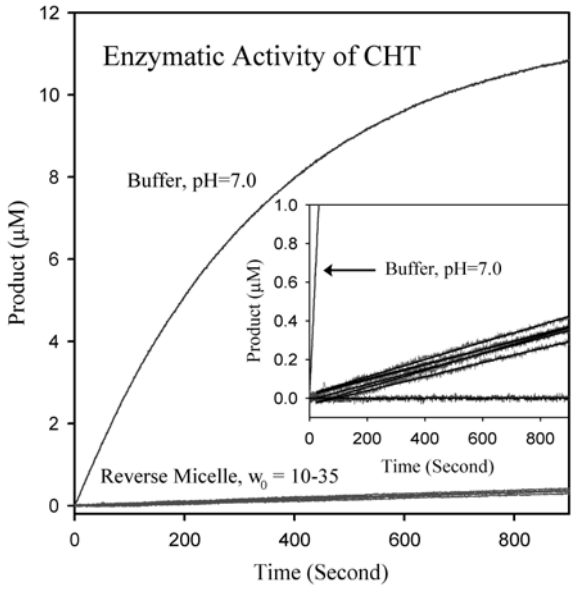

Figure 8. The concentrations of the product as a function of time in *aqueous buffer* and in *reverse micelle* at various degrees of hydration. *Inset* shows that the catalytic rate of the enzyme CHT in reverse micelle is nearly *insensitive* to the degree of hydration. The data points *approximately* horizontal to the time axis indicate that no catalytic reaction has taken place in the absence of the enzyme. The data obtained for buffer at pH 7 is also shown (indicated by an arrow) in the inset for comparison. Kinetic parameters are given in table 1.

concentrations in the RM were 1 μM and 14 μM, respectively. For comparison, enzyme-substrate reaction in aqueous buffer with similar enzyme and substrate concentrations were performed (Figure 8). No reactions were observed in aqueous buffer and RM in the absence of the enzyme.

Role of hydration on enzymatic activity. Figure 7, depicts time dependent product formation (upper) and the Lineweaver-Burk plot (lower), where the reciprocal of the reaction velocity (v) is plotted as a function of the reciprocal of the initial concentration of AMC in the aqueous buffer solution. The linear behavior is appropriate because the kinetics is in the Michaelis-Menten regime where the concentration of the substrate is much higher than that of the enzyme CHT ([E]). This allows one to obtain the dissociation and rate constants, K_m and k_{cat}, respectively. From the slope (K_m/v_{max}; v_{max} is the maximum velocity) and intercept ($1/v_{max}$) of the numerical fitting, the values of K_m and k_{cat} ($v_{max}/[E]$) were found to be 2.53 mM and 4.87 sec^{-1}, respectively. We would like to mention here that one of the early studies[40] of enzyme-substrate kinetics involving same substrate (AMC) reported that the values of K_m and k_{cat} are 0.5 mM and 0.83 sec^{-1}, respectively.

However, information reported in Ref.[40] is rather limiting. The source of the chymotrypsin was not mentioned clearly; being obtained from Worthington

Corporation. The enzyme assays were conducted at 24 ^{o}C (in our case 25 ^{o}C) utilizing 50 mM TES buffer, pH=8.0, containing 10 mM calcium chloride and 1% dimethyl sulfoxide (DMSO) in a final assay volume of 1 ml. The substrate was initially dissolved in 100% DMSO. No kinetic plot or additional information was provided in the article except values for the K_m and k_{cat}. The variation in the experimental conditions is most likely to be the reason for the observed differences between the results reported here and those in Ref[40].

In Figure 8, we show the concentration of the product (measured from the absorbance at 370 nm) as a function of time for different environmental conditions of the enzyme-substrate complex. It is clear from the above figure that the changes in product concentration (obtained from the measured absorbance at 370 nm) in RM are relatively small (*inset* of Fig. 8). However, the variations in slopes are distinguishable even when the absorbance is plotted as a function of time for all the cases studied. In order to obtain the rate of hydrolysis of the substrate AMC by CHT in RM, the extinction coefficients of the free product coumarin were measured at various values of w_0. The extinction coefficients varied approximately linearly in AOT-RM from 11.19 mM^{-1} cm^{-1} at w_0 = 10 to 12.3 mM^{-1} cm^{-1} at w_0 = 35. The velocities of enzymatic reactions estimated from the changes in product concentrations with time, in the aqueous buffer and in RM are tabulated (Table 1). From Table 1 it is clear that in reverse micelle the velocity of enzymatic reaction is about two orders of magnitude slower than that found in the aqueous medium. However, the velocity of the reaction is independent of the degree of hydration (w_0) of the RM.

Given that the global structure of CHT remain almost the same in all the w_0 values studied here (Ref. [16]), the present observation clearly indicates that

Table 1. Velocity (v, μM sec^{-1}) of the catalytic reaction of the enzyme CHT in aqueous *buffer* and *reverse micelle*. The concentrations of the enzyme and the substrate were 1 μM and 14 μM, respectively.

Medium	Velocity (v, μM sec^{-1})
Aqueous Buffer, pH=7.0	2.9×10^{-2}
AOT Reverse Micelle	
w_0 = 10	4.0×10^{-4}
w_0 = 15	4.4×10^{-4}
w_0 = 20	4.0×10^{-4}
w_0 = 25	4.5×10^{-4}
w_0 = 30	3.6×10^{-4}
w_0 = 35	3.8×10^{-4}

the retardation of the enzymatic activity in the RM is *not* due to the structural perturbation of the enzyme in the water pool of the RM. Reaction may also be slowed down through inhibition of active sites in enzyme when it is encapsulated in RM. The active-site titration study mentioned in the Ref[16] indicated that at higher contents, the number of active sites of CHT in AOT-RM is approximately constant at 80% of the value in aqueous solution. The active site concentration of CHT in aqueous solution was measured to be 63% of the total existing catalytic sites[16]. The number of active sites is therefore *not* equal to the total number of catalytic sites (equal to the number of protein molecules) in aqueous solution. Note that approximately 80% (as mentioned in Ref[16]) of the active sites existing in aqueous solution is available for enzymatic reaction in RM. It is therefore expected that the 20% reduction in available catalytic sites compared to that in bulk may not account for the observed retardation of reaction in RM. The cause of the retardation of enzymatic activity in RM is yet to be conclusively determined. Several mechanisms have, however, been conjectured in the literature [[41]and references therein]. These include (i) the lower degree of hydration (compared to aqueous buffer) make the enzyme relatively rigid[37] and decreases its functionality; (ii) the modification of the apparent pK_a at the active site of the enzyme due to polarity changes in the interior water pool; (iii) immobilization of the enzyme due to electrostatic interactions between the enzyme and the surfactant molecules. (iv) distribution of the substrate in RM (interface versus water-pool) and the partitioning of the population of the substrate in the organic and aqueous RM. This may lead to enzyme-substrate complexation less probable.

The distribution of the substrate (at various w_0) is expected to affect the enzymatic activities of CHT in reverse micelle in a very important manner. For example, a larger distribution in the *n*-heptane compared to that in RM might result in an apparent reduction of the activity. However, the substrate studied here is sparingly soluble in bulk *n*-heptane, but soluble in AOT-n-heptane solution. It is therefore unlikely that the majority of the substrate population would reside in the organic phase. Rather, it would like the interface. Our preliminary experiments show a red shift (due to solvatochromism) of about 5 nm only (peak-position) when the environment changes from $w_0 = 0$ to $w_0 = 35$ (highest degree of hydration studied here). This observation, however, cannot specifically indicate whether the substrate is located entirely inside the RM or exploring various layers of water-pool. Dynamical studies coupled with computer simulation will be able to bring out microscopic details of such events. It should be noted here that some of the mechanisms mentioned above could contribute to the enzymatic activity in a positive way, i.e. increase the substrate specificity and/or reduce substrate inhibition and hence increase overall catalytic efficiencies of enzymes[41,42].

For other substrates in the RM involving hydrolysis of N-glutaryl-L-phenylalanine p-nitroaniline, *p*-nitrophenyl acetate and *p*-nitrophenyl caprylate by CHT a bell-shaped dependencies of enzymatic activity on the degree of hydration (w_0) with a maximum around w_0=10 were reported[16,24]. Our studies do not find any significant dependency (Table 1) of the catalytic activity on w_0. Overall enzymatic activity is the convoluted effect of enzyme flexibility (hydration), which is maximum in the aqueous buffer and the efficiency of enzyme-substrate complexation. The present observation of constant catalytic activity on the variation of w_0 reveals that other mechanisms as detailed below have to be taken into account along with the hydration of the enzyme in the RM. First, from X-ray small-angle scattering experiment it has been demonstrated [24] that after inclusion of CHT into the AOT- RM, the enzyme resides in the water pool and *not* at the interface. The study is in agreement with previous reports on the location of CHT as observed by the kinetic decay measurement of hydrated electrons (w_0>20)[43] and fluorescent active-site probing[44].

Given the fact that the size of the enzyme-included water pool increases with w_0[45], any surface affinity of the substrate would expectedly increase enzyme-substrate distance. This will effectively increase the free energy barrier between the enzyme and the substrate. Thus, enhanced flexibility of the enzyme[37] and decreased efficiency of enzyme-substrate complexation with increasing w_0 may make the overall catalytic activity apparently independent of the degree of hydration. Second, in a recent work based on small angle neutron diffraction experiment[46] it has been concluded that there is no variation of protein-filled micellar size except at low hydration level (w_0<5). The conclusion is further supported by time-resolved fluorescent active-site probing[44]. These experimental findings are in contrast to the model described above and depicted in the reference[45] which predicted an almost linear dependence of the core radius of protein-filled micelle with w_0=5-25. Thus, in first approximation one can expect that the enzyme activity will be unaffected at various water content (w_0), because the size of the enzyme-filled droplet is the same in the regime 10<w_0<30[44]. This is consistent with our observation.

3.3. Dynamics of the nanoenvironments: Solvation and Förster resonance energy transfer

In this work we used fluorescence resonance energy transfer (FRET) technique to assess distances of three energy acceptor probe molecules (Two cationic and one anionic) from the surface of the RM before and after encapsulation of CHT. The energy donor, coumarin 500 (C500; neutral) was selectively excited at the RM surface by using specific excitation wavelength. The energy acceptors Rhodamine 123 (R123; cationic), Ethidium Bromide

(EtBr; cationic), Merocyanine 540 (MC540; anionic) being extremely hydrophilic are completely insoluble in the nonpolar phase (isooctane) of the RM. The molecular structure of the donor, acceptors and the surfactant AOT are shown in scheme I. Upon selective excitation, the donor C500 at the RM surface undergoes FRET to the acceptors in the aqueous phase of the RM. By observing the picosecond to nanosecond dynamics of nonradiative energy transfer of the donor in the RM without and with CHT, we elucidate locations of the charged acceptors with respect to the anionic inner surface of the RM. In order to unravel the change in the environmental dynamics around the donor we also studied picosecond resolved solvation dynamics and polarization-analyzed anisotropy of the donor at the surface of the RM without and with CHT.

Solvation and selective excitation of the donor. The donor C500 is sparingly soluble in water and shows reasonably good solubility in isooctane. In bulk water the absorption peak (400 nm) is significantly red shifted compared to that in isooctane (360 nm). The emission peak of C500 in bulk water (500 nm) also shows a 90 nm red shift compared to that in isooctane (excitation at 350 nm). The significantly large solvatochromic effect (solvation) in the absorption and emission spectra of C500 makes the dye an attractive probe for microenvironments. As shown in the figure 9, in isooctane C500 offers significant solubility and the absorption spectrum shows a peak at 360 nm with a shoulder at 380 nm. Upon addition of AOT (w_0=10) another shoulder (at 400 nm) appears in the absorption spectrum, which remains similar for C500 in CHT-included RM (w_0=10) indicating a population of the donor in the polar environment of the RM. The signature of the population of donor molecules in the polar environment of the RM is also evident from the difference spectrum (middle panel of figure 9) of the donor in the RM (w_0=10) with respect to the donor in isooctane. From the absorption spectra it is clear that upon excitation at 400 nm, only that population of donor molecules is excited which are in the polar environment of the RM. The lower panel of figure 9 clearly shows the effect of excitation wavelength on the emission of the donor in the RM. The donor in the AOT/isooctane mixture shows an emission peak at 430 nm with excitation wavelength at 350 nm, indicating emission from both the population of the donor molecules in polar and nonpolar environments. Upon excitation at 400 nm the donor emission is peak shifted to 500 nm revealing the population of donor molecules in the polar environment only. The insignificant change of absorption/emission spectra of the donor with w_0 and upon inclusion of CHT in the RM is not surprising, given the fact that C500 is sparingly soluble in bulk water and expected to reside at the surface of the RM.

Quenching of the donor emission in the reverse micelle. In figure 10 (upper panel) the spectral overlap of the donor (C500) emission and absorption

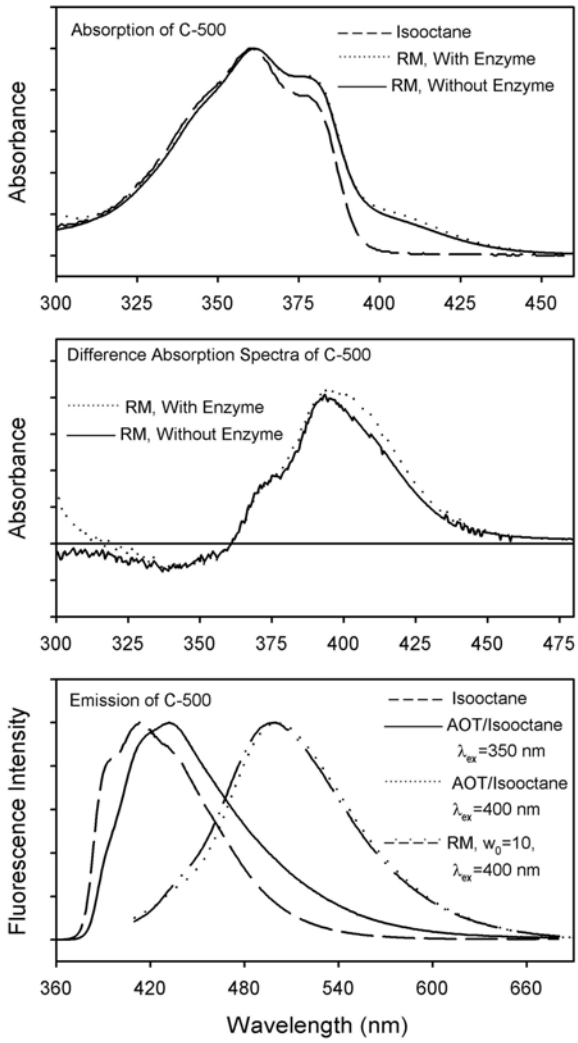

Figure 9. Upper panel shows absorption spectra of C500 (donor) in isooctane and in the RM (w_0=10) without/with the enzyme CHT. Differential absorption spectra of C500 in the RM are shown in the middle panel. A solution of C500 in isooctane, which appears as base line in the spectra is used as reference. From the absorption spectra the signature of the C500 population in the aqueous environments at 400 nm is clearly evident. In the lower panel emission spectra of C500 in nonpolar solvent (isooctane), AOT/isooctane mixture and in the RM (without CHT) with various excitation wavelengths are shown. Note that at excitation wavelength of 400 nm, C500 in the aqueous environments of the RM would selectively be exited.

of R123 (energy acceptor) is shown. The specific property of accumulation in the mitochondria of living cells and the ability of selectively reducing clonal growth of carcinoma cells in vitro makes R123 an attractive probe in biomedical research[47]. The cationic dye R123 being extremely soluble in bulk water and completely insoluble in isooctane makes it a very good reporter of the aqueous phase of a RM. The fluorescence quenching effects of the donor

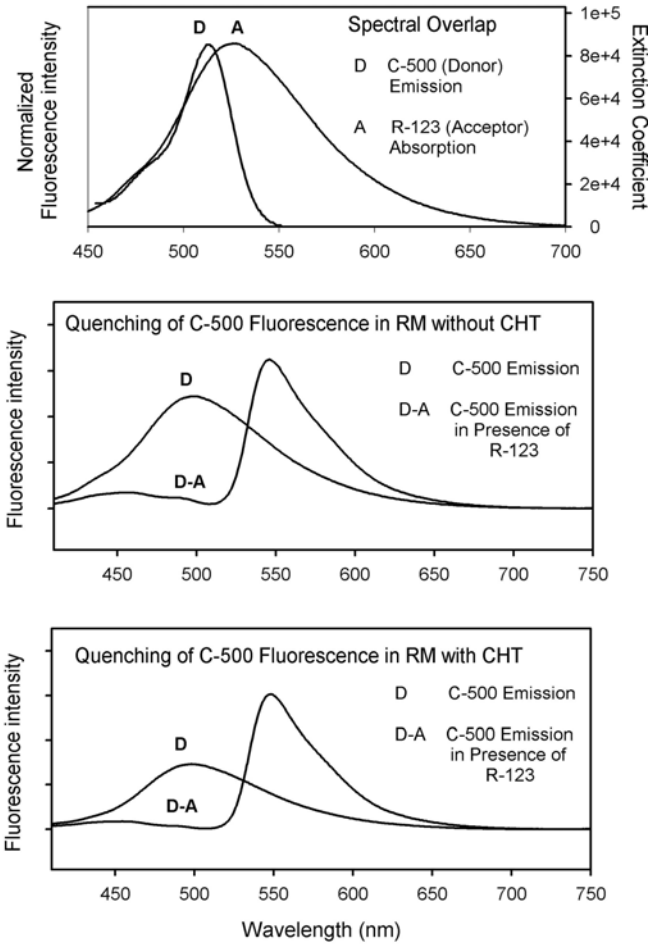

Figure 10. The fluorescence energy transfer processes of C500 (donor) to a cationic acceptor R123 in the RM as evidenced from steady state measurements are shown. In the upper panel the spectral overlap between donor emission and acceptor absorbance is shown. Middle and lower panel show quenching of the donor emission in presence of the acceptor in CHT-excluded and included RM respectively. Estimated parameters are given in the table 2 and table 3.

C500 in the RM without and with CHT by the acceptor R123 are shown in middle and lower panels of figure 10 respectively. In the case of RM without CHT (table 2) the quenching efficiency measured by the ratio F_{DA}/F_D, where F_D and F_{DA} are the emission intensities of the donor in absence and presence of the acceptor, is higher than that in the RM with CHT (table 3). The estimated donor-acceptor distances from steady state experiments in the RM without and with CHT are 31.08 Å and 27.74 Å respectively. Note that in the case of R123 there is a huge disagreement of the donor-acceptor distances measured from steady state and time resolved experiments and would be discussed later.

The spectral overlap of the donor C500 and cationic acceptor EtBr is shown in the upper panel of figure 11. EtBr is a well-known fluorescent probe

Table 2. Energy transfer from C500 (donor) to various acceptors in α-chymotrypsin excluded reverse micelle: Steady state measurement.

Acceptor	Overlap integral ($M^{-1}cm^{-1}nm^4$)	F_{DA}/F_D	R_0 (Å)	R^S (Å)
R123	1.99×10^{15}	0.061	48.97	31.08
EtBr	2.46×10^{14}	0.206	34.56	27.59
Mc540	2.74×10^{15}	0.141	51.65	38.23

Table 3. Energy transfer from C500 (donor) to various acceptors in α-chymotrypsin included reverse micelle: Steady state measurement.

Acceptor	Overlap integral ($M^{-1}cm^{-1}nm^4$)	F_{DA}/F_D	R_0 (Å)	R^S (Å)
R123	2.11×10^{15}	0.028	50.20	27.74
EtBr	2.50×10^{14}	0.471	35.18	34.52
Mc540	2.64×10^{15}	0.353	52.12	47.10

for DNA, which readily intercalates into the DNA double helix. Compared to the case of bulk water, the emission intensity and lifetime of EtBr increase nearly 11 times when EtBr intercalates into the double helix of DNA. This remarkable fluorescence enhancement of EtBr is utilized to study the motion of DNA segments. The photophysical processes of the fluorescence enhancement have recently been explored[48]. The selective accumulation of the acceptor in the aqueous phase of the RM comes from the specific nature of the solubility of EtBr; it is completely insoluble in isooctane and highly soluble in the bulk water. The fluorescence quenching effects of the donor C500 in the RM without and with CHT by the acceptor EtBr are shown in middle and lower panels of figure 11 respectively. In the case of RM without CHT (table 2) the quenching efficiency, F_{DA}/F_D is lower than that in the RM with CHT (table 3). The estimated donor-acceptor distances from steady state experiments in the RM without and with CHT are 27.59 Å and 34.52 Å respectively.

Figure 12, upper shows spectral overlap of the donor C500 emission and acceptor MC540 absorption spectra. MC540 is an anionic lipophilic polymethine dye, which readily binds to biomembranes, micelles, and proteins. In aqueous solutions, the fluorescence intensity of MC540 increases by an order of magnitude on binding to these biological systems. Further, leukamia cells stained with MC540 are rapidly destroyed on irradiation by light. The photophysical processes of the fluorescence enhancement have recently been explored[49]. The selectivity of the acceptor to the aqueous phase of the RM comes from the specific nature of the solubility of MC540; it is completely insoluble in isooctane and highly soluble in bulk water. The significantly large

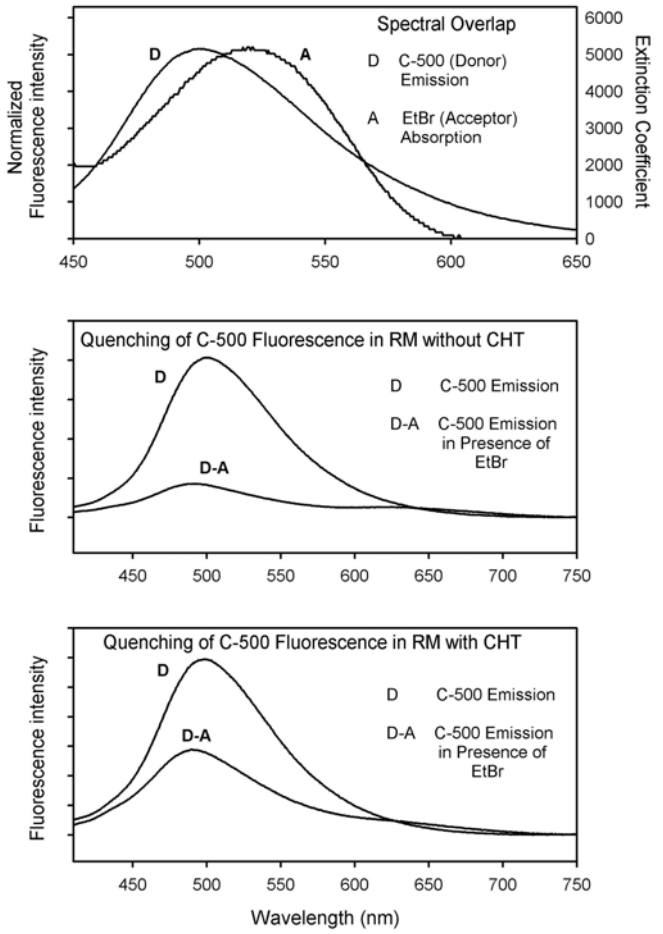

Figure 11. The fluorescence energy transfer processes of C500 (donor) to a cationic acceptor EtBr in the RM as evidenced from steady state measurements are shown. In the upper panel the spectral overlap between donor emission and acceptor absorbance is shown. Middle and lower panel show quenching of the donor emission in presence of the acceptor in CHT excluded and included RM respectively. Estimated parameters are given in the table 2 and table 3.

overlap facilitates quenching of the donor in the donor-acceptor system in RM without and with CHT as shown in the middle and lower panels of figure 12 respectively. In the case of RM without CHT (table 2) the quenching efficiency, F_{DA}/F_D is lower than that in the RM with CHT (table 3). The estimated donor-acceptor distances from steady state experiments in the RM without and with CHT are 38.23 Å and 47.10 Å respectively.

From the steady state quenching studies of the donor C500 it has been revealed that upon inclusion of CHT in the RM the donor acceptor distances for EtBr and MC540 increase. However, in the case of R123 the more efficient quenching of the donor reveals the donor acceptor distance in the case of CHT included RM to be lower than that in the RM without CHT. This observation is

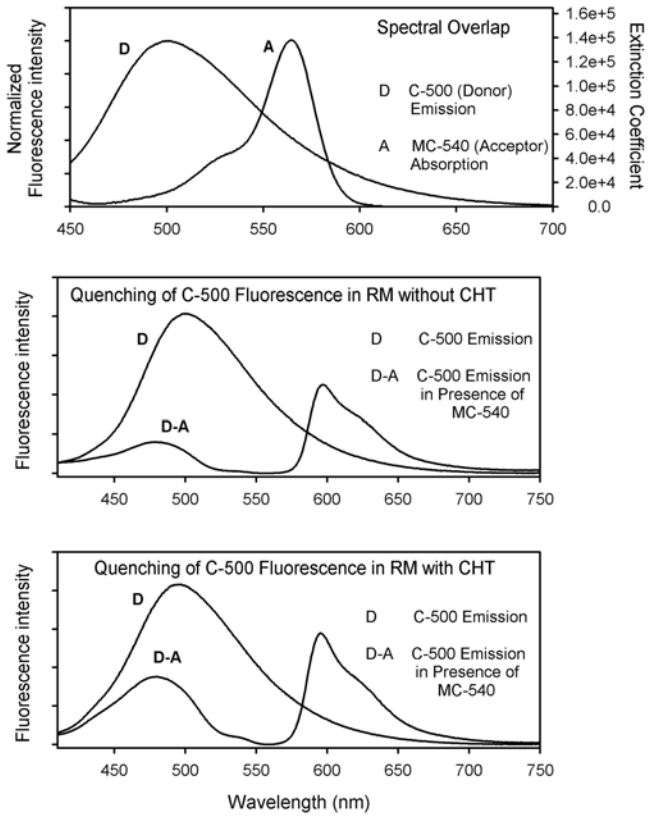

Figure 12. The fluorescence energy transfer processes of C500 (donor) to a anionic acceptor MC540 in the RM as evidenced from steady state measurements are shown. In the upper panel the spectral overlap between donor emission and acceptor absorbance is shown. Middle and lower panel show quenching of the donor emission in presence of the acceptor in CHT excluded and included RM respectively. Estimated parameters are given in the table 2 and table 3.

not in agreement with the time resolved studies as discussed in the following section. The absolute intensity of C500 in the CHT included RM as shown in the middle panels of figures 10,11 & 12 *should not* be compared with that in the RM with CHT (lower panels of figures 10,11 & 12). Because the experimental condition, namely optical density of the probe C500 in the above two cases were different. However, the steady state quenching efficiency (F_{DA}/F_D) does not depend on its absolute intensity. In the cases of donor acceptor systems of R123 and MC540, the acceptors show large emission intensities as shown in the figure 10 and figure 12 respectively. These emissions are *not* due to the direct excitations of the acceptors, because in the excitation wavelength (400 nm) the acceptors offer negligibly small optical absorptions. The enhanced emissions from the acceptors are the indications of energy transfer processes in the RM. In the buffer solution the steady-state spectroscopic studies (absorption, emission and anisotropy; data not shown)

did not reveal any indication of complexation of the acceptors with CHT. However, the possibility of some specific interactions of the acceptor molecules with the RM-encapsulated CHT cannot be completely ruled out for the following reasons. Firstly, the proximities of the acceptors to CHT in the RM are much higher than those in the bulk buffer. Secondly, hydrophobic/charge interactions of CHT with the acceptors could be different compared to those in the buffer because of spatial distribution of pH of the aqueous medium in the RM[48]. Nevertheless, our time-resolved anisotropy studies, which reflect the spatial restriction on the acceptor molecules (see below) in the CHT-included/excluded RM, indicate negligibly small interactions of the acceptor molecules with CHT upon encapsulation in the RM. Thus within the structural integrity of the enzyme in the RM, it is most expected that in the CHT-included RM, acceptors reside in the interstitial space between the enzyme surface and the inner surface of the RM.

Solvation and rotational dynamics of the donor at the reverse micellar surface. In order to explore the local environmental rigidity and its change upon inclusion of the enzyme CHT, we studied solvation dynamics of the RM by using the donor as probe in absence and presence of CHT. Figure 13 (upper) shows the picosecond-resolved transients of the donor C500 in the RM without CHT at three characteristic wavelengths. For solvation dynamics studies a series (at least 7) of systematic wavelengths were taken. The signal initially decays with time constants 200 ps and 1.0 ns at the blue side (~ 425 nm) of the fluorescence spectrum but rises with similar time constant at red side (~ 625 nm). A decay component for all wavelengths were found with a time constant of ~5 ns as shown in figure 13, upper. The slower 5 ns component is the fluorescence lifetime of the probe C500 in the microenvironment.

The constructed time resolved emission spectra (TRES) are shown in figure 13, lower. The steady-state spectrum of C500 in the RM is also shown for comparison (dotted line). The solvation correlation function C(t) (figure 14 and table 4) shows single-exponential decay with time constant of 645 ps; any sub-50 ps components in these dynamics are unresolved. The net spectral shift ($\Delta\nu$) is 1889 cm^{-1} from 21755 cm^{-1} to 19866 cm^{-1} (up to 3.0 ns). The anisotropy r(t) of the donor is shown in the inset of figure 14. The measured r(t) decays with time constants 210 ps (36%) and 1.2 ns (51%) resulting a persistency (13%) of r(t) in our experimental window (up to 10 ns). The value of r(t) at t=0 is found to be 0.39.

Figure 15, upper shows picosecond-resolved transients of the donor C500 in the CHT included RM. On the blue edge of the fluorescence spectrum the signals decay with time constants (240 ps-1.1 ns) depending on wavelengths, whereas on the red edge the signals are seen to rise (time constant up to 1.1 ns).

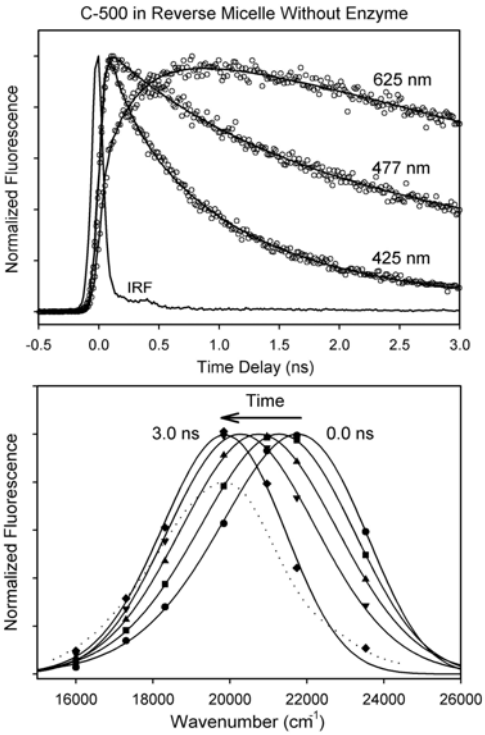

Figure 13. In the upper panel picosecond resolved transients of the C500 in the CHT-excluded RM are shown at three characteristic wavelengths. Note the decay in the blue edge (425 nm) and the rise in the red edge (625 nm) of the emission spectrum. Solid lines show numerical fitting of those transients. Instrument response function (IRF) is also shown. The transients are normalized for comparison. Lower panel shows time-resolved emission spectra (TRES) of C500 in the RM. Steady-state spectrum of the sample is also shown for comparison (dotted line). Note that the emission maximum at time 3 ns is similar to that of the steady state emission.

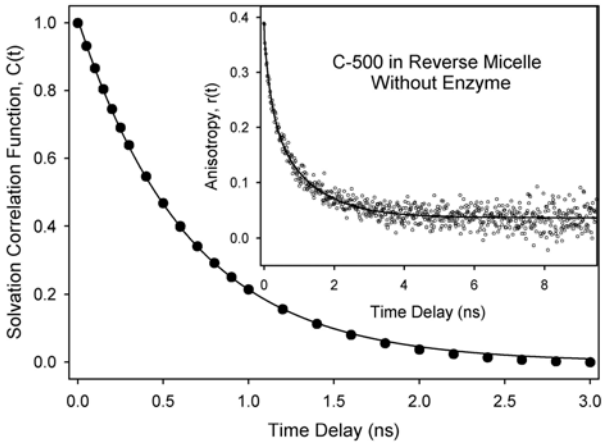

Figure 14. Solvation correlation function, $C(t)$, of C500 in the CHT excluded RM. *Inset* shows the time-resolved anisotropy, $r(t)$ of C500 in the same system. Numerical fitting parameters are given in the table 4.

Table 4. Numerical fitting parameters of the time resolved solvation and anisotropy of donor and donor-acceptor systems in the RM.

Reverse Micelle	Emission Maximum (nm)	Solvation Correlation Function, C(t)	Rotational Anisotropy, r(t)
α-cymotrypsin-excluded	500	Single exponential decay τ= 645 ps $\Delta\nu$=1889 cm^{-1}	r_0=0.39 τ_1=0.21 ns, A_1=36% τ_2=1.2 ns, A_2=51% Residual r(t)=13%
α-chymotrypsin-included	500	Single exponential decay τ= 668 ps $\Delta\nu$=1412 cm^{-1}	r_0=0.40 τ_1=0.43 ns, A_1=44% τ_2=1.7 ns, A_2=33% Residual r(t)=23%

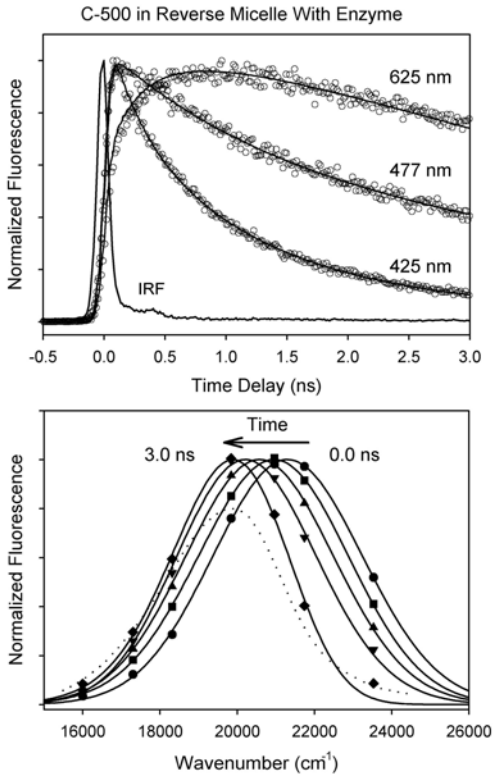

Figure 15. In the upper panel picosecond resolved transients of the C500 in the CHT-included RM are shown at three characteristic wavelengths. Note the decay in the blue edge (425 nm) and the rise in the red edge (625 nm) of the emission spectrum. Solid lines show numerical fitting of those transients. Instrument response function (IRF) is also shown. The transients are normalized for comparison. Lower panel shows time-resolved emission spectra (TRES) of C500 in the RM. Steady-state spectrum of the sample is also shown for comparison (dotted line). Note that the emission maximum at time 3 ns is similar to that of the steady state emission.

A decay component, of time constant 5 ns reflective of lifetime of the probe is present in all wavelengths detected (figure 15, lower). Figure 15, lower shows TRES (up to 3.0 ns) of the donor in the CHT included RM. The dotted spectrum indicates the steady-state spectrum of the donor. The C(t) function in figure 16, can be fitted to a single-exponential decay with time constant of 668 ps; any sub-50 ps components in these dynamics are unresolved (table 4). The net spectral shift is 1412 cm^{-1} from 21301 cm^{-1} to 19889 cm^{-1} (up to 3.0 ns), which is similar to that of the RM without CHT. As shown in the inset of figure 16, the fluorescence anisotropy r(t) at 500 nm decays exponentially with time constants of 434 ps (44%) and 1.7 ns (33%). In contrast to the RM without CHT the anisotropy at t=0 (0.4) and relatively large residual anisotropy (23%; up to 10 ns) reveal slower rotational dynamics of the probe in the RM upon inclusion of the enzyme CHT.

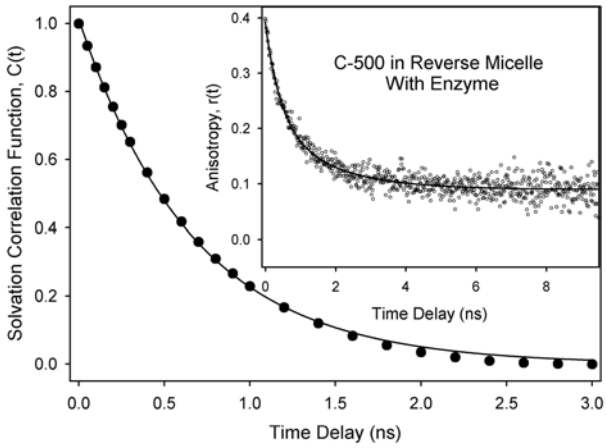

Figure 16. Solvation correlation function, *C*(*t*), of C500 in the CHT included RM. *Inset* shows the time-resolved anisotropy, *r*(*t*), of C500 in the same system. Numerical fitting parameters are given in the table 4.

Heterogeneity in the local environments of the donor. To investigate possible interference of emission from various excited species, we further use time resolved area normalized emission spectroscopic (TRANES) technique developed recently[30]. Figure 17 shows TRANES spectra of the donor in the RM without (upper) and with CHT (lower). An isoemissive point at 21000 cm^{-1} is clearly evident in the spectra of both the samples. One of the possible reasons of existence of two emissive species in the excited state is due to the solubilization of the C500 chromophore in two different sites of the RM[30]. In other words the environments around the donor in the RM are heterogeneous.

Diffusion of the probe donor through various environments: Emission line-width analysis. The full-width at half maxima (line widths; Γ) of emission

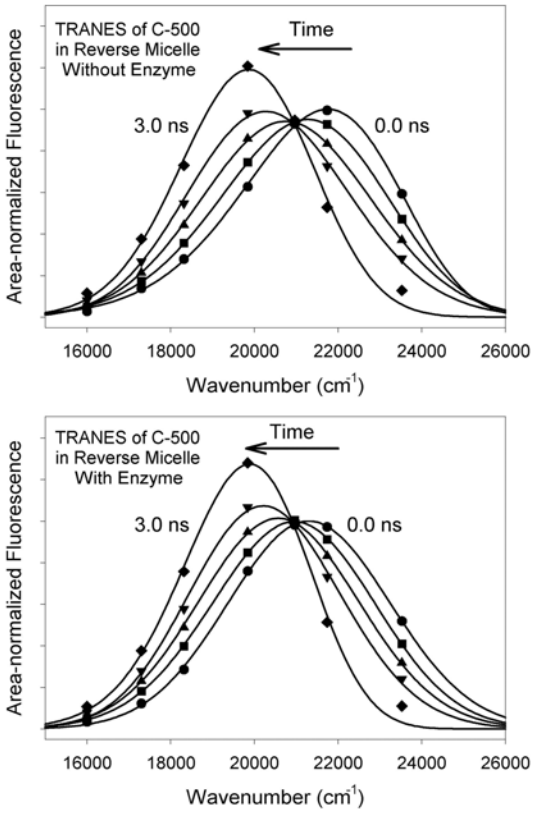

Figure 17. Time-resolved area normalized spectra (TRANES) of C500 in the CHT excluded (*upper*) and in the CHT included (*lower*) RM. Note the isoemissive points at 21000 cm^{-1} for both the systems (see text).

spectra of the C500 probe (figure 9, lower) were observed to be different in various environments. It increases upon changing the polarity of the immediate environment of C500. In the RM, w_0=10, the emission line width of C500 is larger than that in pure isooctane. The line width of emission of C500 in the RM is also very sensitive to inclusion of the enzyme CHT. In the RM without CHT the magnitude of the Γ (3845 cm^{-1}) is larger than that in the CHT included RM (3606 cm^{-1}). The observation is consistent with the fact that in the polar environment, the fluorescence spectrum of a solute (C500) with higher excited state dipole moment compared to that in ground state is the superposition of emission from different excited states of diverse degrees of solvation[29]. The broadening of emission spectrum may also be indicative of spatial microheterogeneity of the immediate environment of the probe C500[50-52].

The line width (Γ) of TRES (figure 18) of C500 in the RM is found to vary with time, which is an evidence of change in local environment during solvation. In the RM without CHT (figure 18) Γ(t) exhibits a relatively faster rise and a slower decay with time constants 322 ps and 1.6 ns respectively. The amplitudes of the rise and decay components of line width (ΔΓ) are 342 cm^{-1}

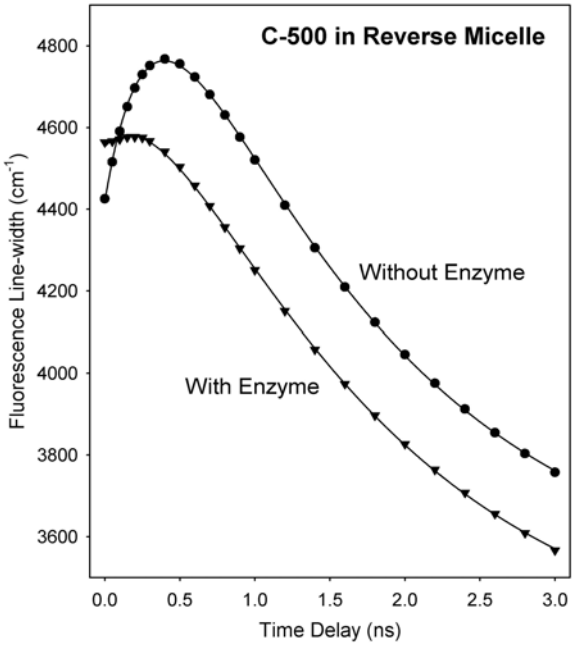

Figure 18. Time-resolved line widths (Γ) of TRES of C500 in the RM without (*up*) and with (*down*) the enzyme CHT are shown. Note the significantly large amplitude of the rise component in the line width with time for the RM without CHT compared to that in the RM with CHT.

(up to 400 ps; from 4426 cm^{-1} to 4768 cm^{-1}) and 1010 cm^{-1} (up to 3.0 ns; from 4768 cm^{-1} to 3758 cm^{-1}) respectively. For the CHT included RM Γ(t) shows similar temporal characteristics, however, the amplitude of the rise component is much smaller than former case. In the latter case the amplitudes of rise (time constant 410 ps) and decay (time constant 1.6 ns) components of line width (ΔΓ) are 13 cm^{-1} (up to 200 ps; from 4564 cm^{-1} to 4577 cm^{-1}) and 1010 cm^{-1} (up to 3.0 ns; from 4577 cm^{-1} to 3567 cm^{-1}) respectively.

From the studies of time dependent spectral width an interesting feature of the relaxation dynamics of C500 in the RM is evident. In the case of the RM without CHT the rise with time constant 322 ps is indicative of diffusion of the probe from the surface of the RM to polar aqueous and nonpolar isooctane phases of the RM making the spatial environments of the donor more heterogeneous with time. After certain time (up to 400 ps) the probe is expected to cross the aqueous phase and again face the nonpolar isooctane medium offering relatively homogeneous environments as evidenced by the decay of the Γ(t). Taking diffusion constant of an organic probe at the micellar surface to be 15.3 $Å^2/ns$[20], the estimated distance traversed by the probe in 400 ps is 3.5 Å. This is much shorter than the diameter of the RM (40 Å) at w_0=10. Conversely, in the CHT included RM the available aqueous phase (shell) for the diffusion of the donor probe is much less than that of the former case. The

estimated distance traveled by the donor in 200 ps is 2.5 Å. As indicated by the magnitude of the rise, the population of the donor molecules in this journey is significantly lower than former case of RM without CHT. The similarity in the amplitudes and time constants of the decay components for both the cases is not surprising, given the fact that these decays are associated with the diffusion of the donor in the nonpolar isooctane medium.

Fluorescence resonance energy transfer of the donor in the RM. In figure 19 the transients of the donor C500 without and with different acceptors in the RM in absence of CHT are shown. As shown in the table 5 and table 6 the fluorescence transient of the donor in the RM shows a fast rise (time constant 200 ps), indicating solvation, followed by a decay of time constant 5.0 ns, which is the lifetime of the donor in the microenvironment. In presence of the acceptor R123 time resolved fluorescence shows biexponential decay of time constants 500 ps (35%) and 4.5 ns (65%). The persistence of the longer lifetime (4.5 ns; 65%) distinctly indicates that in the donor-acceptor system only 35% of the donor population is undergoing energy transfer process[28]. The estimated donor-acceptor distance is 33.98 Å. From the biexponential transient of time constants 1.1 ns (40%) and 4.6 ns (60%) of C500-EtBr system in the RM it is evident that 40% of the donor population is responsible for the energy

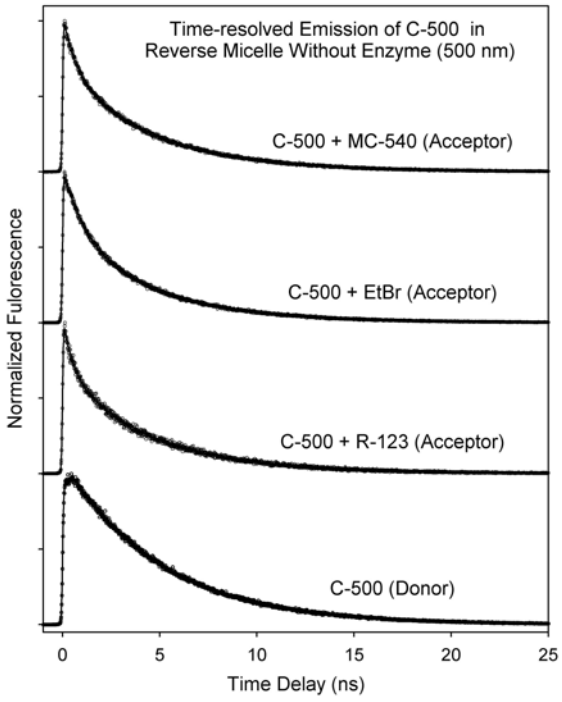

Figure 19. Time-resolved transients of the donor (C500) in the CHT-excluded RM in absence and presence of various acceptor molecules are shown. All the transients were taken at 500 nm and normalized for comparison. Numerical fitting parameters are given in the table 5.

Table 5. Numerical fitting parameters of the transients of donor and donor-acceptor systems in the CHT excluded RM

System	a_1 (%)	τ_1 (ns)	a_2 (%)	τ_2 (ns)	τ_{DA}/τ_D	R^{TR} (Å)
Donor	-32	0.2	132	5.0	-	-
Donor-Acceptor						
R123	35	0.5	65	4.5	0.100	33.98
EtBr	40	1.1	60	4.6	0.218	27.94
MC540	35	0.72	65	4.7	0.144	38.37

Table 6. Numerical fitting parameters of the transients of donor and donor-acceptor systems in the CHT included RM.

System	a_1 (%)	τ_1 (ns)	a_2 (%)	τ_2 (ns)	τ_{DA}/τ_D	R^{TR} (Å)
Donor	-28	0.2	128	5.0	-	-
Donor-Acceptor						
R123	-30	0.2	130	4.9	~1	-
EtBr	38	1.0	62	4.7	0.200	27.92
MC540	26	0.76	74	4.8	0.152	39.14

transfer with an average distance of 27.94 Å from the acceptor EtBr. In the case of C500-MC540 system the biexponential decay of the donor fluorescence reveals two time constants of 720 ps (35%) and 4.7 ns (65%). This indicates that 35 % of the donor molecules in the RM transfer their energy to acceptors at an average distance of 38.37 Å. The efficiency of the energy transfer for various donor-acceptor systems and estimated average donor acceptor distances are summarized in table 5. All estimated distances in the RM without CHT are less than the diameter of the water pool (40 Å) of the RM at w_0=10.

Figure 20 shows fluorescence transients at 500 nm of the donor C500 in the CHT-included RM in absence and presence of various acceptors. The fluorescence transient of the donor in this case shows a fast rise (time constant 200 ps), indicating solvation, followed by a decay of time constant 5.0 ns, which is the lifetime of the donor in the RM. In presence of the acceptor R123 a significant quenching of emission of the donor is evidenced by steady state measurement (figure 10) and also by the poor signal to noise ratio of the acquired transient (figure 20, second from bottom). However, the transient is similar to that of the donor in absence of the acceptor, indicating the quenching to be reflective of a radiative mechanism of energy-transfer (re-absorption by the acceptor) *not* the resonance type. In contrast to the former case, the lack of coexistence of donor and acceptor in the CHT included RM is the possible reason

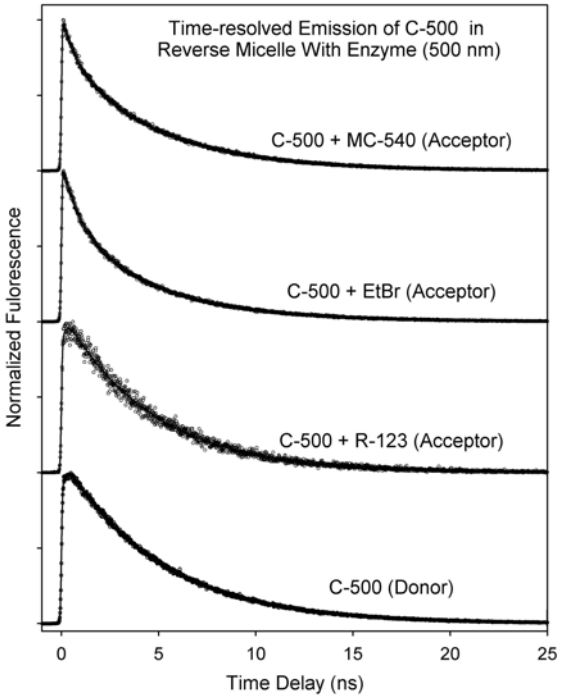

Figure 20. Time-resolved transients of the donor (C500) in the CHT-included RM in absence and presence of various acceptor molecules are shown. All the transients were taken at 500 nm and normalized for comparison. Numerical fitting parameters are given in the table 6.

for the radiative energy transfer mechanism. The disagreement of the estimated donor-acceptor distances from steady state (table 3) and time resolved studies (table 6) warrant a potential danger of using the former as a conclusive experiment to measure donor-acceptor distance by using the energy transfer mechanism in chemical and biological systems. From the biexponential transient of time constants 1.0 ns (38%) and 4.7 ns (62%) of C500-EtBr system in the RM it is evident that 38% of the donor population is responsible for the energy transfer with an average distance of 27.92 Å from the acceptor EtBr. In the case of C500-MC540 system the biexponential decay of the donor fluorescence reveals two time constants of 760 ps (26%) and 4.8 ns (74%), which indicate 26 % of the donor molecules in the RM transfer their energy to acceptors at an average distance of 39.14 Å. The estimated distances are similar to that in the RM without CHT except for the acceptor R123, where the distance is too large to have resonance type energy transfer in the CHT included RM.

Local environmental restriction on the acceptors. In order to explore the local geometric restriction of the microenvironment on the physical motions of the acceptors in the RM without and with CHT we performed time resolved anisotropy studies (r(t)) of the acceptors. In these studies we excited

the donor molecule and measured the anisotropy at the peak wavelengths of the acceptor molecules. In the CHT-excluded (figure 21) and included (figure 22) RM fluorescence anisotropy decays of the acceptors (r(t)) could be described by bi-exponential functions. The time constants, relative amplitudes and residual anisotropy values are shown in the table 7. The fast depolarization components can be attributed to the local tumbling motions of the acceptors. The slow component, which is similar to the donor molecules in the corresponding RM, can tentatively be assigned to a rotation of the whole molecule and/or global rotational motion of the RM.

The similarity in the transients of anisotropy of the acceptor molecules in the CHT-included RM with that in RM without CHT is reflective of analogous

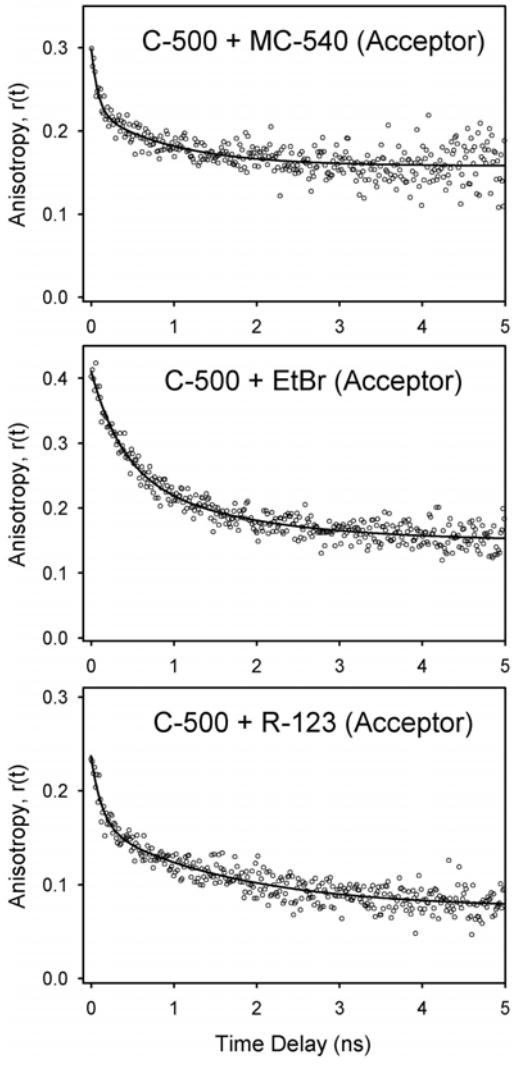

Figure 21. Time-resolved anisotropies of the acceptor molecules, MC540 (upper), EtBr (middle) and R123 (lower) in the CHT-excluded RM are shown. Note that acceptors were excited indirectly (via donor). Numerical fitting parameters are given in the table 7.

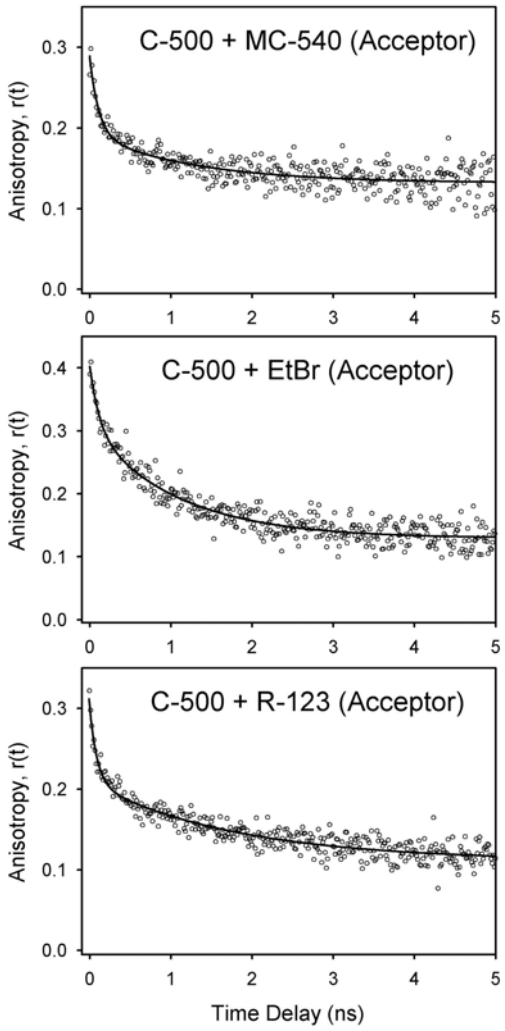

Figure 22. Time-resolved anisotropies of the acceptor molecules, MC540 (upper), EtBr (middle) and R123 (lower) in the CHT-included RM are shown. Note that acceptors were excited indirectly (via donor). Numerical fitting parameters are given in the table 7.

Table 7. The time-resolved anisotropy of the donor C500 and donor-acceptor systems in Reverse Micelle.

Reverse Micelle	Donor (C500)	C500-R123	C500-EtBr	C500-MC540
CHT Excluded	r_0=0.39 τ_1=0.21 ns, a_1=36% τ_2=1.2 ns, a_2=51% Residual r(t)=13%	r_0=0.23 τ_1=0.13 ns, a_1=30% τ_2=1.7 ns, a_2=40% Residual r(t)=30%	r_0=0.40 τ_1=0.37 ns, a_1=38% τ_2=1.5 ns, a_2=30% Residual r(t)=32%	r_0=0.30 τ_1=0.10 ns, a_1=27% τ_2=0.98 ns, a_2=23% Residual r(t)=50%
CHT Included	r_0=0.40 τ_1=0.43 ns, a_1=44% τ_2=1.7 ns, a_2=33% Residual r(t)=23%	r_0=0.30 τ_1=0.10 ns, a_1=30% τ_2=1.9 ns, a_2=32% Residual r(t)=38%	r_0=0.40 τ_1=0.12 ns, a_1=24% τ_2=1.1 ns, a_2=45% Residual r(t)=31%	r_0=0.27 τ_1=0.11 ns, A_1=35% τ_2=1.3 ns, A_2=22% Residual r(t)=43%

geometrical restriction on the acceptors in the microenvironments. This observation is consistent with the fact that the interactions of acceptor molecules with CHT in the RM are not significant. Note that the anisotropy values at t=0 (r_0) and the faster time constants of the acceptor molecules in the CHT-excluded/included RM may have interference from the energy transfer dynamics from the donor molecule. From the data given in the table 5, table 6 and table 7, it is evident that the faster time constants (0.1-0.4 ns) in the anisotropy decays are faster than those of the characteristic time constants of energy transfer processes (0.2-1 ns) and the slower time constants are comparable in both cases. This observation is consistent with the significant randomization of relative orientation between donor and acceptor molecules prior to or during the energy transfer process.

4. α-chymotrypsin in cetyltrimethylammonium bromide (CTAB) micelle

4.1. Structure of α-chymotrypsin upon interaction with CTAB micelle

In our studies, we have used dansyl chromophore (DC)[26] covalently attached to CHT. This labeling is well known[26,53,54] to occur mostly at ε-amino groups of the lysine and arginine residues exposed at the enzyme surface within the overall structural integrity of the enzyme. There are ten such sites in CHT, as depicted by stick-model in figure 23, upper. Early studies[55,56] on the covalent attachment of the dansyl probe to CHT found that there is a certain possibility of sulfonation of the active site of the enzyme. In such cases, one *cannot* expect *functional intactness* upon the labeling of the dansyl chromophore to the enzyme. The FTIR absorbance spectra of CHT in the absence and in the presence of CTAB micelles shows insignificant differences (Figures 23a and 23b)[5]. The secondary structure change is confirmed by the difference spectrum presented in Figure 23(c). Seven component bands are resolved in the free CHT spectrum (Figure 23a). As described in the reference[5] the maximum absorption is centered at 1637 cm^{-1}, indicating a protein structure with a high content of anti-parallel *β*-sheet. The two bands at 1622 and 1673 cm^{-1}can be attributed to low- and high-frequency components of *β*-sheet, whereas the band centered at 1655 cm^{-1} corresponds to α-helix conformation. The component at 1647 cm^{-1} is assigned to unordered segments, and the bands at 1665 and 1685 $cm^{-1}$are attributed to *β*-turns[57]. The resolved components and the determined 62% *β*-sheet content are in agreement with previous IR studies of CHT[57]. Upon binding to CTAB micelles, the main component centred at 1637 cm^{-1}, assigned to *β*-sheet is still present (Figure 23b). Although the secondary structure of CHT is mainly retained, there is a

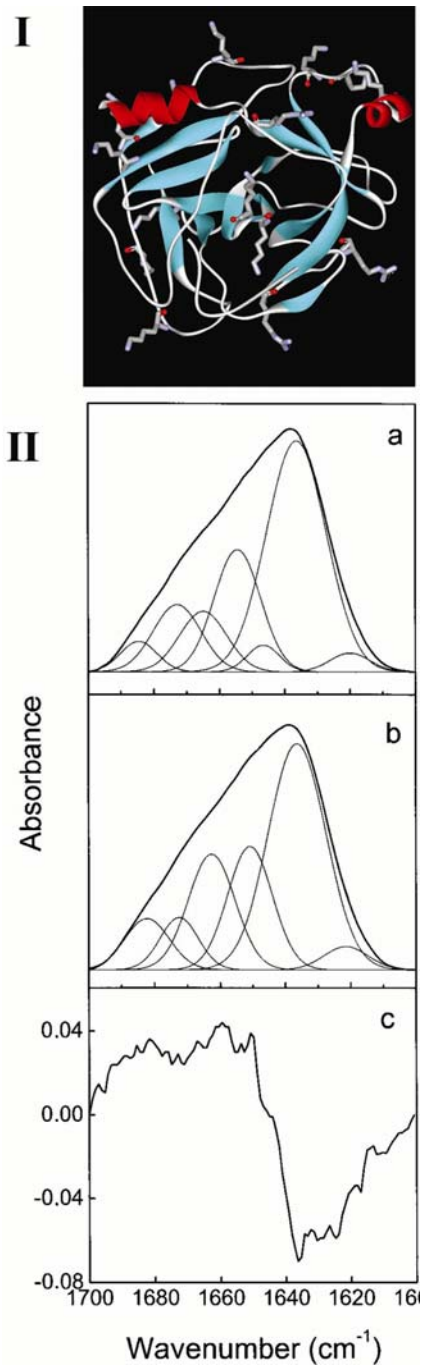

Figure 23. (I) Ten potential sites of α-chymotrypsin for the binding of the probe DC (lysine and arginine residues) are shown by *stick* model. (IIa) FTIR absorption spectra of 267 μM CHT in 20 mM tris/HCl buffer, where Gaussian curves are the spectral components obtained by curve fitting. (IIb) as in (a) for CHT in the presence of 3 mM CTAB micelles, taken after 2 h equilibration. (IIc) Difference spectrum obtained by subtracting a normalized spectrum of free protein from a normalized spectrum of micelle-bound protein (×100). Similar results were found with 30.0 mM CTAB. Reprinted with permission from reference [5]. Copyright 2004 biochemical society.

reduction in β-sheet content and the disappearance of the component corresponding to unordered structure. The decrease in β-sheet is accompanied by an increase in the bands corresponding to α-helix and turns. These changes are also illustrated by the difference spectrum shown in Figure 23(c), where the normalized spectrum of free protein is subtracted from that of micelle-bound protein. The positive band above 1650 cm^{-1} indicates a higher content of α-helix and turns structures on bound CHT, and the negative band below 1650 cm^{-1} suggests that the interaction with micelles reduces the unordered and β-sheet content. Therefore the FTIR study reveals a small increase in the α-helix content together with a small reduction in β-structure of CHT.

4.2. Dynamics at the micellar surface

In this work we have used DC as an extrinsic probe at the CTAB micellar surface in order to investigate the solvent dynamics and local rigidity around the micelle. Upon UV excitation, in polar media dansyl chromophore undergoes a twisted intramolecular charge transfer (CT) reaction[53,58]. For non-polar solvents, in the steady state, the emission is strong and is mostly from locally excited (LE) state (i.e. before charge separation). In polar solvents, the fluorescence decreases and is dominated by emission from the CT state. The solvent polarity and rigidity of the environment around the probe determine the wavelength and yield of emission. That is why dansyl is a useful biological probe. A molecular picture of solvation for the probe has been detailed in reference[53]. The study used femtosecond resolved laser spectroscopic technique and confirmed that in polar solvent, upon UV excitation the probe undergoes a CT reaction along with reorganization of solvent molecules around the probe (solvation). In the bulk polar solvent and with the protein Histone I, the time scale of twisting (8-11 ps) was found to be longer than that of solvation (<1 ps). Thus it was concluded that during the transformation from the initial LE state to the CT state, the polar solvent can "immediately" respond to the new configuration of the solute.

For bulk polar solvents it is known that there is a time scale separation between the CT reaction and solvation dynamics[53], the former being an order of magnitude slower than later. However, if the two processes are having comparable time scale, particularly in a biomolecular environment, the use of DC as a probe of solvation dynamics requires further cautions. The important point is to find out if a probe undergoing a twisted CT reaction in the excited state is suitable for interrogating the environmental relaxation (solvation) or not. Secondly, if there is a different emissive species due to CT reaction in the excited state, whether it is possible to get the signature of the species. To address the above-mentioned questions, we have studied a cationic micelle

(cetyltrimethylammonium bromide, CTAB) using dansyl chromophore (scheme I) as a fluorescent probe. The micelle is often used to mimic the surface effect of proteins[53,59-61]. However, the dynamical time scale of the environmental relaxation at micellar surface is significantly different from that at the protein surfaces[54]. By observing picosecond to nanosecond dynamics of population and polarization-analyzed anisotropy for the micelle-probe complex, we elucidate the nature of local environmental relaxation and the rigidity of binding structure of the complex. To confirm the coexistence of LE and CT excited states in the emission of the dansyl probe we also used time-resolved area-normalized emission spectroscopic (TRANES) method[30-32].

Solvation of the dansyl chromophore. Figure 24 shows steady-state emission spectra of dansyl probe in various environments. At the surface of an enzyme α-chymotrypsin (CHT) dansyl (covalently bound) shows a fluorescence peak at 564 nm. For the dansyl-bonded enzyme and the CTAB-micelle complex, the emission maximum shifts to 547 nm. The fluorescence spectrum of dansyl probe with the CTAB micelle shows a peak at 484 nm. In all the cases the excitation wavelength was maintained at 400 nm. The emission spectrum of the dansyl chromophore in bulk *n*-heptane, a nonpolar solvent is also shown for comparison. Fluorescence maximum at 457 nm (excitation at 350 nm) is obtained, which is 27 nm blue shifted compared to that in the micellar environment. From the steady-state spectra, the solvatochromic shift of the fluorescence towards longer wavelengths with the increase in environmental polarity is evident (see below).

In a micellar solution, there are three possible locations of the probe, bulk water, inner hydrocarbon core and the peripheral stern layer (at the surface).

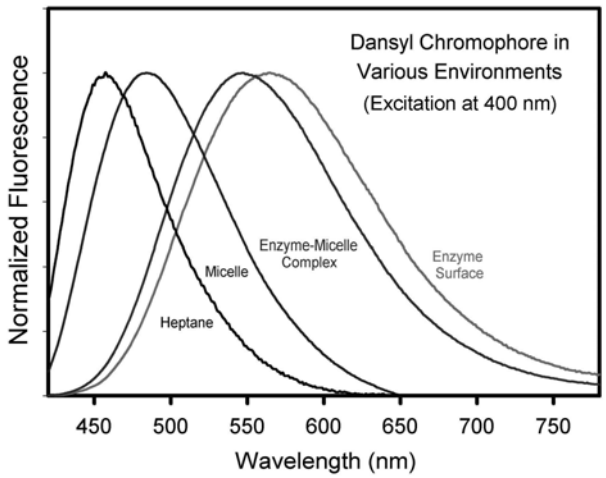

Figure 24. The normalized steady state fluorescence spectra of the probe dansyl in chemical and biological environments (see text). Note the huge solvatochromic shift in emission.

Dansyl is sparingly soluble in water and after solubilization in micelle the time-resolved anisotropy, r(t) shows a decay (see below) which is much slower than that in bulk solvent (~50 ps)[53], revealing a clear indication of the attachment of the probe with the micelle. Thus the first possibility can be ruled out. In the hydrocarbon core the emission maximum is expected to be similar to that in *n*-heptane, which is not the case here. Moreover dansyl molecules staying in the non-polar hydrocarbon core of the micelle is not expected to contribute to the observed solvation dynamics. Thus the dynamics is exclusively due to the dansyl molecules at the surface stern layer.

The transients observed at three characteristic wavelengths, from the blue to the red side of the fluorescence spectrum of dansyl in the micelle, are shown in Figure 25. The emission transients detected in the blue region of the fluorescence spectrum are characterized by an instant rise (instrument response function, IRF) and a picosecond decay component (~350 ps). When detection is done in the red region, the decay part slows down until eventually an initial rise on a picosecond time scale (~350 ps) is observed. A nanosecond decay was found to be almost 12 ns, which is present at all wavelengths with different contributions is the lifetime of dansyl chromophore in the relaxed equilibrium state[53]. These overall features are well recognized as being characteristics of solvation[59].

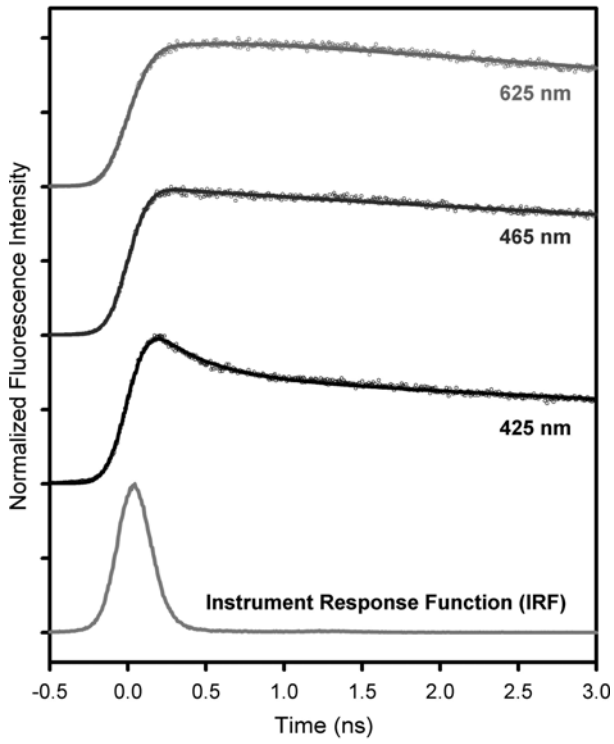

Figure 25. Picosecond-resolved transients at three characteristic wavelengths of the dansyl probe in micelle. Transients are normalized for comparison.

Figure 26 depicts the TRES curves of dansyl in the CTAB micelle. The steady-state fluorescence spectrum is shown in the figure 26 (dotted line) for comparison with infinite time (2 ns in this case) spectrum. The time evolution of C(t) is shown in figure 27. The decay curve of the C(t) was fitted to an exponential function, giving a time constant of 338 ps where the 50 ps or less component was not resolved. The net dynamical spectral shift is 374 cm^{-1} (from 20441 cm^{-1} to 20067 cm^{-1}) over a time span of 2 ns. The temporal behavior of the C(t) is very similar to the dynamics observed recently using the

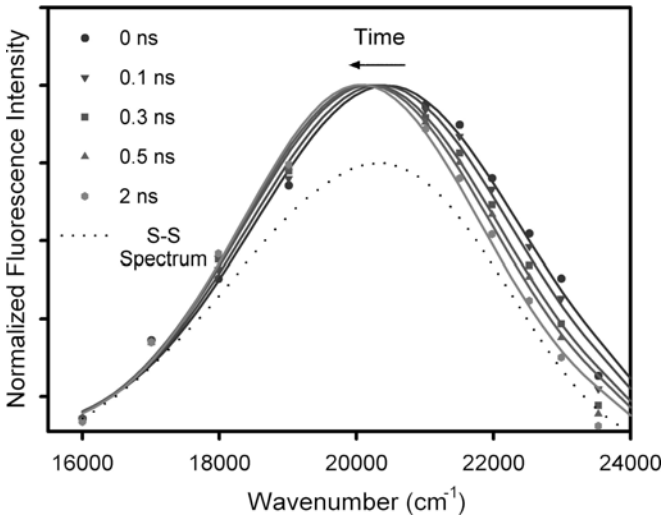

Figure 26. The normalized spectral evolution (TRES) at five delay times from t=0 for dansyl in the micellar environment. The dotted line indicates steady-state spectrum of the probe dansyl in micelle.

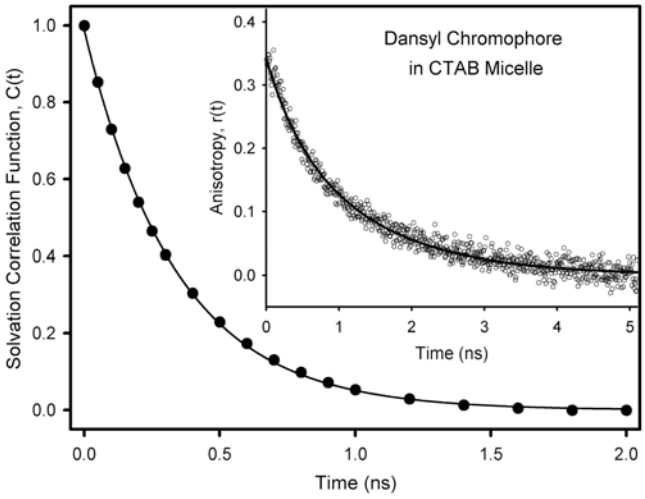

Figure 27. The solvation correlation function, C(t) of the micellar environment probed with the dansyl chromophore. Inset shows time-resolved anisotropy, r(t) decay of the dansyl probe in the micellar environment.

DCM (4-(dicyanomethylene)-a-methyl-6(p-dimethylaminostyryl) 4H-pyran) as solvation probe[59]. The study[59] reported a biexponential nature of the decay of C(t) with time constants 170 ps (50%) and 630 ps (50%); estimated average solvation time and net spectral shift were found to be 400 ps and 550 cm^{-1} respectively, consistent with our observations.

Solvation vs. twisting dynamics. To study the degree of orientational rigidity of the dansyl probe in the micelle and the nature of spectral shift in the solvation process, we obtained the fluorescence anisotropy decay at the wavelength 488 nm for the excitation wavelength of 405 nm. The anisotropy, r(t) function is the sum of two exponentials (inset of figure 27) with time constants 413 ps (23%) and 1.3 ns (77%) with r(t)=0.34 at t=0 ns. The faster time constant (413 ps; 23%) is similar to the solvation time constant 338 ps obtained from C(t) decay. Thus an entanglement of conformational changes, which should alter the anisotropy to yield twisted CT state in the observed solvation dynamics can not be completely ruled out. However, lesser weight (23%) of the faster time constant (413 ps) of the r(t) decay and resemblance of the observed time constant of solvation dynamics with other study[59] using a different probe DCM reveal that the contribution of conformational dynamics (twisting) to the solvation is *not* significant. The longer time constant (1.3 ns; 77%) could be due to rotational diffusion of the DC chromophore at the micellar surface and/or slow tumbling motion of the micelle as a whole.

Existence of excited CT state. As mentioned above there is an indication of existence of excited twisted CT in the time resolved emission. To ascertain emission from two excited states, we further followed time-resolved area-normalized emission spectroscopy (TRANES)[30-32]. Figure 28 shows TRANES spectra of dansyl chromophore in the CTAB micelle. An isoemissive point at

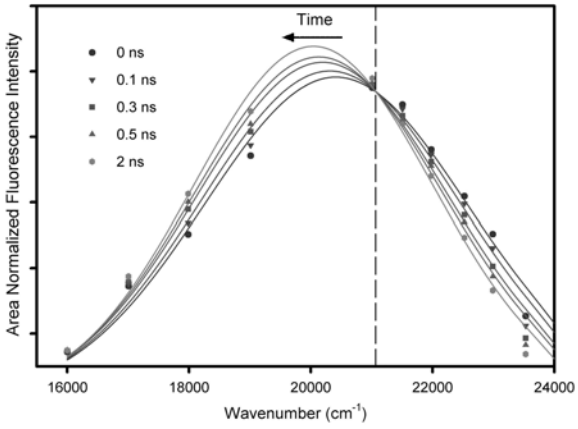

Figure 28. Time resolved area normalized emission spectra (TRANES) of the dansyl probe in micellar environment at five delay times from t=0 ns. Note the isoemissive point at 21066 cm^{-1} (see text).

21066 cm^{-1} is clearly evident in the spectra. One of the possible reasons of existence of two emissive species in the excited state (as indicated by the isoemissive point in the TRANES spectra) is due to the solubilization of the dansyl chromophore at two different sites of the micelle[31]. However, our observation of entanglement of conformational dynamics with the solvation and other steady-state study reported in the reference[58] support the coexistence of the excited CT state with the LE state (before charge transfer).

4.3. Dynamics and functionality of the enzyme-micelle complex

Here we present our studies on the picosecond resolved solvation dynamics at the surface of an enzyme bovine pancreatic α-chymotrypsin (CHT) in free buffer and that of its complex with a cationic cetyltrimethylammonium bromide (CTAB) micelle. The CHT-micelle complex is important to mimic the possible influence of *crowding* [62,63] or confinement of the enzyme in its *real* physiological working environment. Extensive studies[5] of the CHT-micelle complex indicate that interfacial binding interaction to the CTAB micelle increases the activity of the enzyme by a factor of 2.5 (at 20 mM CTAB concentration) compared to that in bulk water (buffer). The study concluded that the higher catalytic activity results from significant conformational change of the micelle-bound enzyme.

The dansyl chromophore (DC) undergoes a twisted intramolecular charge transfer (CT) in the excited state to generate the fluorescing state[53,58], and the process of solvation leads to continuous red shift of the emission spectrum. These dynamics are also determined by solvent relaxation[53]. Our studies also use time resolved area normalized (TRANES) spectra of DC, in order to check the emission from the CT state of the probe DC during the process of solvation. By observing the picosecond to nanosecond dynamics of population and polarization analyzed anisotropy for the enzyme-micelle complex, we elucidate the nature of local solvation and polarity at the surface of CHT and binding structure of the complex.

Enzymatic Activity. Activity measurements of CHT in CTAB micelle were performed using Ala-Ala-Phe-7-amido-4-methyl-coumarin (AMC) as the substrate. Concentration of the substrate in aqueous buffer was estimated on taking extinction coefficient value at 325 nm (ε_{325}) to be 15.9 $mM^{-1}cm^{-1}$. The enzyme cleaves the substrate and produces a free coumarin derivative. The absorbance of the coumarin derivative was monitored in the spectrophotometer. A cell of 1 cm path length was used for measurements both in aqueous buffer (pH 7.0) and the micelle. The enzyme concentration was 1.0 μM. The micelle-bound enzyme-substrate reactions were started by the addition of an aliquot of the stock aqueous buffered substrate solution to the pre-equilibrated micelle-CHT complex in buffer solution at 25°C. The initial

concentration of AMC was maintained in excess to that of the enzyme and was varied over a wide range. The increase in absorption at 370 nm due to the release of 7-amido-4-methyl-coumarin (in the micellar solution the extinction coefficient of the product at 370 nm was measured to be ε_{370}=13.4 mM^{-1} cm^{-1}) was followed[4] as time progresses. Note here that the substrate does not absorb at this monitoring wavelength. Initial rates were measured in the regime where the absorbance varies *linearly* with time. The reaction followed the Michaelis-Menten kinetics[39]. The apparent K_m and k_{cat} values were derived by least squares fitting of the double reciprocal Lineweaver-Burk plot (see below).

Figure 29, upper shows time dependent product concentration as a result of enzymatic activity of CHT in CTAB micellar environment ([CTAB]=50 mM, pH=7.0). For comparison we also show the enzymatic behavior in free buffer (pH=7.0). For both the cases the enzyme and substrate concentrations were maintained to be 1 μM and 334 μM respectively. Figure 29, lower depicts the Lineweaver-Burk plot, where the reciprocal of the reaction velocity (v) is plotted as a function of the reciprocal of the initial concentration of AMC in the aqueous buffer solution. From the slope (K_m/v_{max}; v_{max} is the maximum velocity) and intercept ($1/v_{max}$) of the numerical fitting. The values of K_m and k_{cat} ($v_{max}/[E]$) were found to be 0.38 mM and 0.1 sec^{-1}, respectively.

This work indicates that the micelle-bound CHT presents 7 times lower catalytic efficiency (k_{cat}/K_m) than the free enzyme. Recent studies[5] of micelle-bound enzyme-substrate kinetics involving the substrate *p*-nitrophenyl acetate (PNPA) reported the values of K_m and k_{cat} to be 29.7 μM and 101 sec^{-1} respectively in presence of 20 mM CTAB. It was also found that the micelle-bound enzyme had 2.5 times higher catalytic efficiency than that of the free enzyme in buffer. However, the study confirmed decrease in enzymatic activity with higher (more than 20 mM) CTAB concentrations and concluded to be due to unfavorable partition of the substrate into the micelle.

In contrast, another study involving a substrate N-glutaryl-L-phenylalanine p-nitroaniline[7] found an opposite effect with CTAB micelle where 20% decrease on the original CHT (in free buffer), which is qualitatively in agreement with our observation. Recently, theoretical models were developed[6] for the treatment of reaction rates of an enzyme in the micellar environments. These models consider both the partitioning of the substrate and the ion exchange at the micellar interface. Three pseudophases: free water, water bound at the micellar surface and that in the micellar core have also been considered in these models. The models predict that the reaction rate of the enzyme exhibits a bell-shaped dependence of surfactant concentration when enzyme-micelle interactions are included in the formulation of the model. The bell-shaped

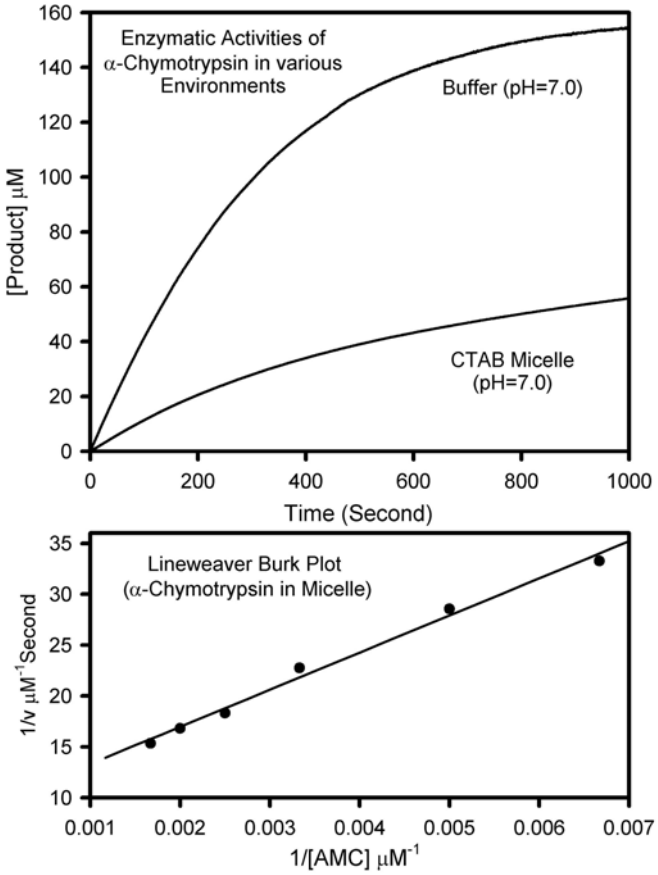

Figure 29. *Upper:* Comparison of the activity of the enzyme CHT in free buffer with that in micellar solution. The rate of product formation in *aqueous buffer* is slower than that in *micellar solution* (see text and table 8). For both the samples enzyme and initial substrate concentrations were maintained at 1 μM and 150 μM respectively. *Lower:* Lineweaver-Burk plot of the enzyme CHT showing its catalytic activity with substrate AMC in the micellar solution at pH = 7.0. The solid line is a linear fit following Michaelis-Menten kinetics.

dependence of reaction rate of CHT on CTAB concentration is recently found in the literature[5].

Location of the substrate and product. The interaction of the substrate with the micellar surface, which leads to partitioning of the substrate into aqueous and micellar phases[5,6] is important points to understand the activity of micelle-bound CHT. A significant affinity of the substrate to the micellar surface essentially decreases the activity of the enzyme CHT with higher CTAB surfactant concentration (above CMC) due to unfavorable partitioning of the substrate into micelle[6]. On the other hand, for optimum activity of a micelle-bound enzyme, the product must have minimum affinity to the micellar surface in order to create space for the substrate by leaving the active site of the enzyme at the micellar surface. Thus it is important to know the

immediate environments of the free substrate and product in the micellar solution in absence of the enzyme. In figure 30 we show dependence of emission intensities of the substrate (upper) and product (lower) on the concentration of the surfactant (CTAB). We further compare intensities of the probes (substrate and product) in solvents (water-ethanol mixture) with different polarities without micelle. Inset figures show changes of relative intensities of the probes in water-ethanol mixture with various ethanol concentrations. The shifts of the maxima of emission spectra of the substrate and product were found to be very small (3-5 nm) toward blue wavelength upon decreasing the polarity of the mixture solution by adding more ethanol (from 0 to 100%). Hence, the solvatochromism and intensity change of the substrate and the product are *not* good probes for their local environmental information.

However, the steady-state anisotropy studies of the substrate and product give some information about their locations in the micellar solutions as evidenced from figure 31. The measured steady-state anisotropy value for the

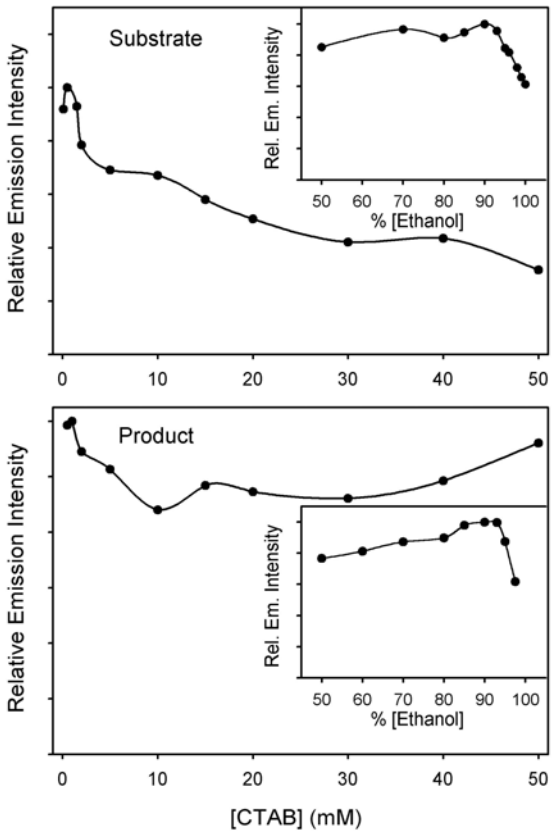

Figure 30. Dependence of emission intensities of the substrate (*upper*) and product (*lower*) on the concentration of the surfactant (CTAB). *Insets* show changes of relative intensities of the probes (substrate and product) in water-ethanol mixture with various ethanol concentrations.

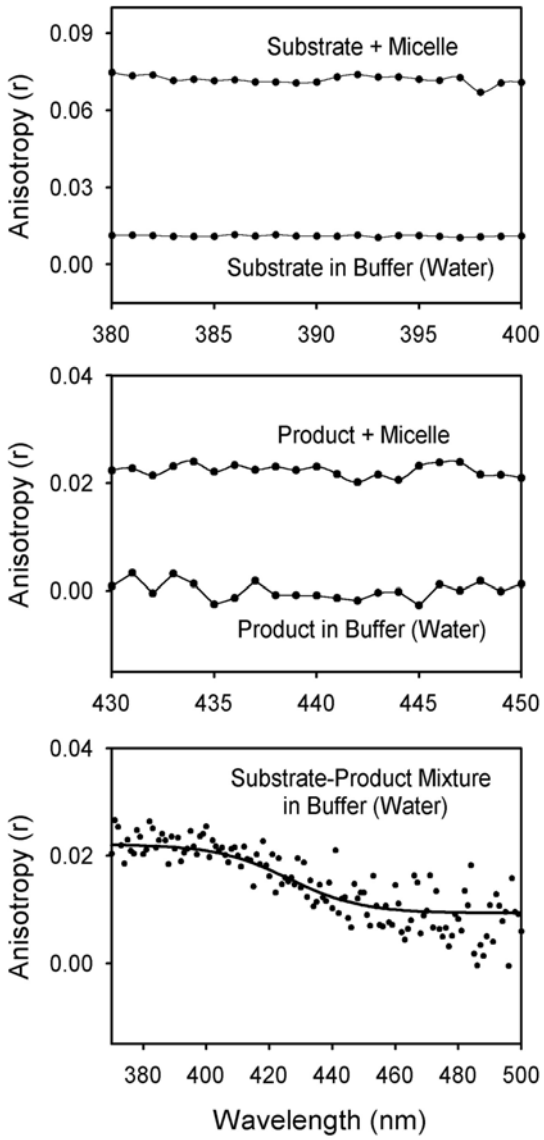

Figure 31. Steady-state anisotropies of the substrate (*upper*) and the product (*middle*) in free buffer and in micellar solution. *Lower panel* shows steady-state anisotropy of the mixture of substrate and product in free buffer (see text).

substrate in aqueous 50 mM CTAB solution is higher (r=0.08) than that of the product (r=0.02) indicating stronger favorable interaction of the substrate with the micelle compared to that of the product. The critical micellar concentration (CMC) of CTAB in the buffer (0.1 M phosphate) was measured by using a fluorescent laser dye DCM (data not shown) and found to be ~ 0.8 mM. For comparison the anisotropy values of the substrate (upper panel) and product (middle panel) in free buffer were also shown. We found a small difference between the anisotropy values of substrate and product in free buffer. Relatively higher anisotropy of the product in the micellar solution (middle

panel) compared to that in free buffer indicates an attractive interaction of the product with the micelle. As the emission peaks of the substrate (390 nm) and product (440 nm) are well separated, in a substrate-product mixture solution a long-range wavelength scanning of steady-state anisotropy is expected to show the signature of both solutes in the solution, which is clearly evident from the lower panel of figure 31.

From the earlier report it was evident that CTAB micelle-bound CHT had tendency to react with the free substrate in the aqueous phase[5] rather reacting with micelle-bound substrate. The affinity of the micelle-bound CHT is similar to that of a matrix enzyme[64]. The observed decrease in activity in our experiment, which is in contrast with the superactivity found in the study[5] can be explained by the unfavorable partitioning of the substrate for its affinity to the micelle and/or finite attractive interaction of the product to the micellar environment as evidenced from the anisotropy study.

Dansyl-bonded CHT in free buffer: Dynamics of solvation. Figure 32 (upper) shows the picosecond-resolved transients of DC attached to CHT with a series of systematic wavelength detection. The signal initially decays with time constant 150 ps at the blue side of fluorescence but rises with similar time constant at red side. Two decay components for all wavelengths were found with a time constant of ~2 ns and 8 ns as shown in figure 32, upper. The observed decay component (2 ns) could be due to charge transfer dynamics[53,58] at the protein surface. The slower 8 ns component is the fluorescence lifetime of the probe DC in the protein environment. Note that at the micellar surface (relatively nonpolar) DC shows fluorescence lifetime of 12 ns and complete absence of the 2 ns decay component[15].

The constructed time resolved emission spectra (TRES) are shown in figure 33, upper. The steady-state spectrum of DC-CHT adduct is also shown for comparison (dotted line). The solvation correlation function C(t) (figure 33, lower) shows single exponential decay with time constant of 142 ps; any sub-50 ps components in these dynamics are unresolved. The net spectral shift ($\Delta\nu$) is 74 cm^{-1} from 17064 cm^{-1} to 16990 cm^{-1} (up to 700 ps). Note that for DC at the micellar surface[15] we recovered $\Delta\nu$ to be 374 cm^{-1} from 20441 cm^{-1} to 20067 cm^{-1} (up to 2 ns). For DC bonded CHT-micelle complex the values of $\nu(0)$ and $\Delta\nu$ are found to be 19397 cm^{-1} and 1068 cm^{-1} respectively (see below). The smaller magnitude of $\Delta\nu$ and significantly large red shifted $\nu(0)$ for DC labeled CHT in buffer compared to those either at the micellar surface[15] or in the CHT-micelle interface, clearly indicates a considerably large *missing* dynamics in our observed C(t) decay. This is not surprising given that time scale of dynamics (hydration) at the surface of proteins in buffer is 20-40 ps [[35]and references therein], which is beyond our experimental resolution. However, our observations are complimentary to those studies with femtosecond resolution.

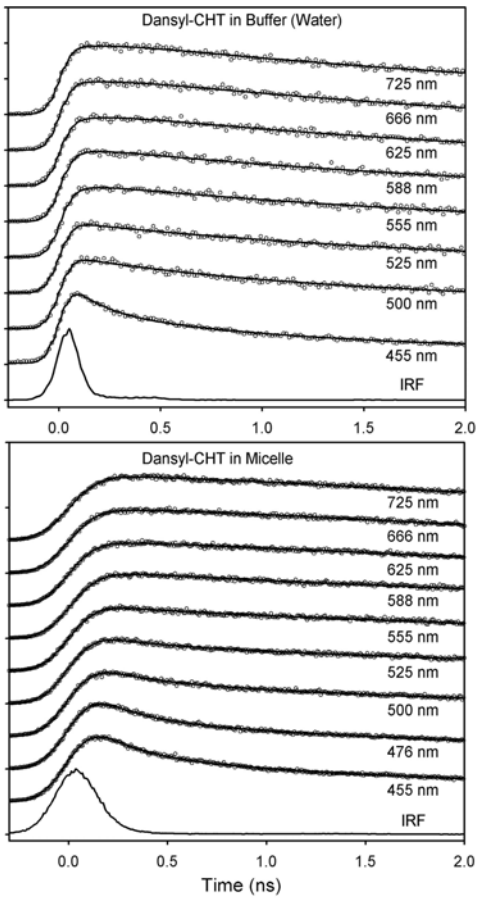

Figure 32. Picosecond resolved transients of the DC-CHT adduct (*upper*) and DC labeled CHT-micelle complex (*lower*). Instrument response functions (IRF) for both the set of transients are shown. The transients are normalized and baseline shifted for comparison.

The anisotropy r(t) of DC attached to CHT is shown in the inset of figure 33 (lower). The measured r(t) decays with time constants 690 ps (20%) and ~47 ns (80%) resulting a persistency of r(t) in our experimental window (up to 10 ns). The value of r(t) at t=0 is found to be 0.38. The dynamics of r(t) which corresponds to the structural relaxation of the probe DC at the protein surface is drastically different from that in bulk methanol, observed with femtosecond resolution[53]. In methanol, the two major components of r(t) decay have time constants 14 ps (40%) and 50 ps (50%), except for small initial decay (10%) which corresponds to the structural relaxation from ultrafast solvation. However, at the micellar surface[15] DC probe shows different dynamics of r(t). The decay of r(t) almost merges exponentially the baseline in 5 ns experimental window with time constants of 413 ps (23%) and 1.3 ns (77%). When DC is covalently connected to CHT, the huge residual anisotropy up to 10 ns indicates restriction of the orientational relaxation due to the anchoring at the protein surface.

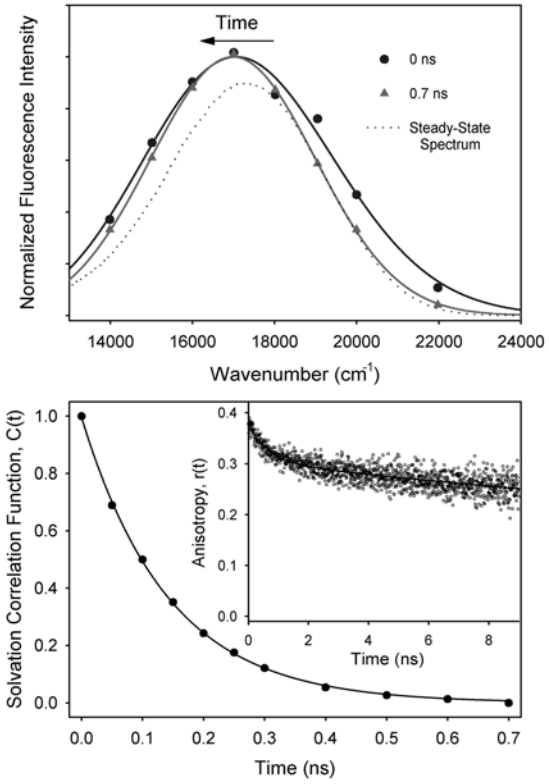

Figure 33. *Upper:* Time-resolved emission spectra (TRES) of the probe DC at the enzyme surface. Steady-state spectrum of the sample is also shown for comparison (dotted line). *Lower:* Solvation correlation function, $C(t)$, of DC at the enzyme surface. *Insets* shows the time-resolved anisotropy, $r(t)$, of DC in the same system.

Enzyme-micelle complex. Figure 32, lower shows picosecond-resolved transients of the DC bonded CHT-micelle complex in aqueous buffer solution. On the blue edge of the fluorescence spectrum the signals decay with time constants (150-250 ps) depending on wavelengths, whereas on the red edge the signals are seen to rise (time constant up to 1.0 ns). A decay component of time constants ~2 ns and a relatively long ~12 ns decay component reflective of lifetime of the probe are present in all wavelengths detected (figure 32, lower). Figure 34, upper shows TRES (up to 2.4 ns) of the complex in aqueous buffer. The dotted spectrum indicates the steady-state spectrum of the complex. It is evident that equilibrium (steady-state) spectrum requires further time to reach, consistent with the longer time scale for post-solvated activated CT in DC[53].

The C(t) function in figure 34, lower can be fitted to a biexponential decay with time constants of 150 ps (65%) and 500 ps (35%); any sub-50 ps components in these dynamics are unresolved. The net spectral shift is 1068 cm^{-1}; from 19397 cm^{-1} to 18329 cm^{-1} (up to 2.4 ns). The shift is much larger than that of the CHT without micelle, indicating significantly smaller *missing*

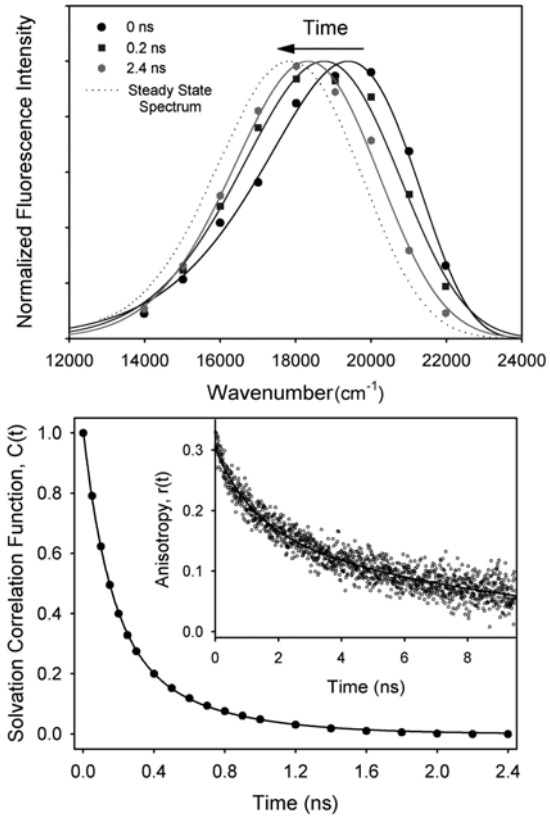

Figure 34 *Upper:* Time-resolved emission spectra (TRES) of the probe DC in the enzyme-micelle complex. Steady-state spectrum of the sample is also shown for comparison (dotted line). *Lower:* Solvation correlation function, $C(t)$, of DC in the enzyme-micelle complex. *Insets* shows the time-resolved anisotropy, $r(t)$, of DC in the same system.

dynamics with our experimental resolution. The faster time constant of 150 ps is similar to the solvation time 142 ps of CHT without micelle, reflective of the probe environments and not that of the CHT-micelle interface. However, longer time constant of 500 ps (35%) is considerably slower than that of either CHT in bulk buffer (142 ps) or micellar surface (374 ps), indicative of an environment at the interface between CHT and the micelle.

As shown in the inset of figure 34, lower the fluorescence anisotropy r(t) at 555 nm decays exponentially to almost baseline with time constants of 1.2 ns (40%) and 8.5 ns (60%). In contrast to the enzyme without micelle the anisotropy at t=0 (0.3) and significantly small residual anisotropy (up to 10 ns) reveal faster rotational dynamics of the probe DC upon complexation with the micelle. The change in the dynamics is consistent with the perturbation of surface structure of the enzyme (CHT) upon complexation with the CTAB micelle, as evidenced from other studies using circular dichroism and FT-IR spectroscopy[5].

Existence of two species. As mentioned in the previous sections, a decay component of time constant of 2 ns is present in all detected transients (figure 32) for DC-CHT in free buffer and with the micelle. The decay of similar time constant (2 ns) for both the samples we studied could be a manifestation of existence of excited twisted CT state. To ascertain possible entanglement of emission from two states (locally excited (LE) and CT states) we further use time resolved area normalized spectroscopic (TRANES) technique[30]. Figure 35 shows TRANES spectra of dansyl chromophore attached to CHT without (upper) and with micelle (lower). An isoemissive point at 19000 cm^{-1} is clearly evident in the spectra of both the samples. One of the possible reasons of existence of two emissive species in the excited state is due to the solubilization of the dansyl chromophore in two different sites of the micelle[30]. However, our observation of entanglement of conformational dynamics with the solvation and other steady-state study reported in the reference[58] support the coexistence of the excited CT state with the LE state (before charge transfer).

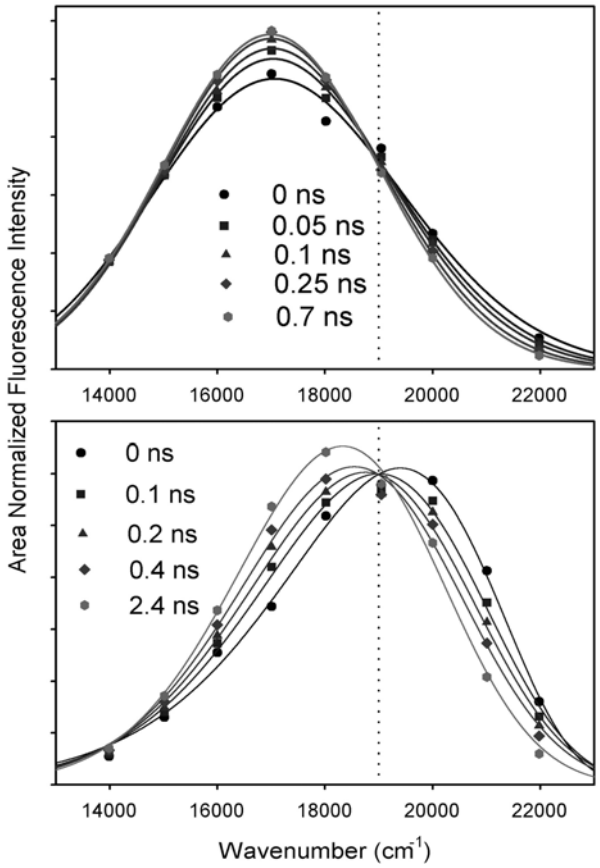

Figure 35. Time-resolved area normalized spectra (TRANES) of DC at enzyme surface (*upper*) and in the enzyme-micelle complex (*lower*). Note the isoemissive points at 19000 cm^{-1} for both the systems (see text).

Diffusion of the probe DC through various environments: Emission line-width analysis. The full-width at half maxima (line widths; Γ) of emission spectra of the DC probe (figure 24) were observed to be different in various chemical and biological environments. The line width increases upon changing the polarity of the immediate environment of DC. In *n*-heptane (nonpolar), micellar surface, enzyme-micelle interface and at the surface of CHT the values of Γ were found to be 3671 cm^{-1}, 4261 cm^{-1}, 4460 cm^{-1} and 4553 cm^{-1} respectively. The observation is consistent with the fact that in the polar environment fluorescence spectrum of a solute (DC) with higher excited state dipole moment compared to that in ground state is the superposition of emission from different excited states of diverse degrees of solvation[29]. The broadening of emission spectrum may also be indicative of spatial microheterogeneity of the immediate environment of the probe DC[50-52].

The line width (Γ) of TRES (figure 36) of DC is found to vary with time, which is an evidence of change in local environment during solvation. At the enzyme surface (figure 36, upper) Γ(t) exhibits a fast decay with time constants 60 ps (80%) and 250 ps (20%). Total change of line width (ΔΓ) is 714 cm^{-1} (up to 700 ps; from 5439 cm^{-1} to 4725 cm^{-1}) which is 13% of the width at t=0. At the micellar surface (figure 36, middle) Γ(t) shows a single exponential decay with time constant 525 ps. The net change of ΔΓ is 345 cm^{-1} (up to 2 ns; from 4986 cm^{-1} to 4641 cm^{-1}) that is 10% of the spectral line width at t=0. In the case of DC at the interface between CHT and micelle, Γ(t) exhibits a fast initial rise (time constant 90 ps) followed by biexponential decay with time constants 120 ps and 3.6 ns (figure 36, bottom). The net ΔΓ of the rise component (up to 150 ps; from 4689 cm^{-1} to 4880 cm^{-1}) is 191 cm^{-1}. For the decay component the net ΔΓ is observed to be 368 cm^{-1} (up to 2.4 ns; from 4880 cm^{-1} to 4512 cm^{-1}).

From the studies of time dependent spectral width an interesting feature of relaxation dynamics of DC in the enzyme-micelle interface is evident. The fast rise with time constant 90 ps is an indicative of diffusion of the probe DC from nonpolar to polar environment. The time constant is also similar to the case of DC at the surface of CHT (60 ps). Conversely, in the latter case the faster time constant of 60 ps results a decay that is an indication of polar to nonpolar diffusion. In the interface the rise-decay characteristics of Γ(t) is one of the clear indications of scanning of the interfacial environment by the probe DC. Most expectedly, the probe first diffuses from the surface of CHT (nonpolar) to the relatively polar (interface) region and then further diffuses to the vicinity of the micellar surface (nonpolar). A similar dynamical characteristics is supposed to be evidenced from the time dependence of r(t). The instrumental resolution (~50 ps) is close to the time scales of the faster dynamics and could be possible cause for the missing dynamics of r(t). However, the slower component of Γ(t) (3.6 ns) is close to the faster ns component (1.2 ns) of r(t) decay.

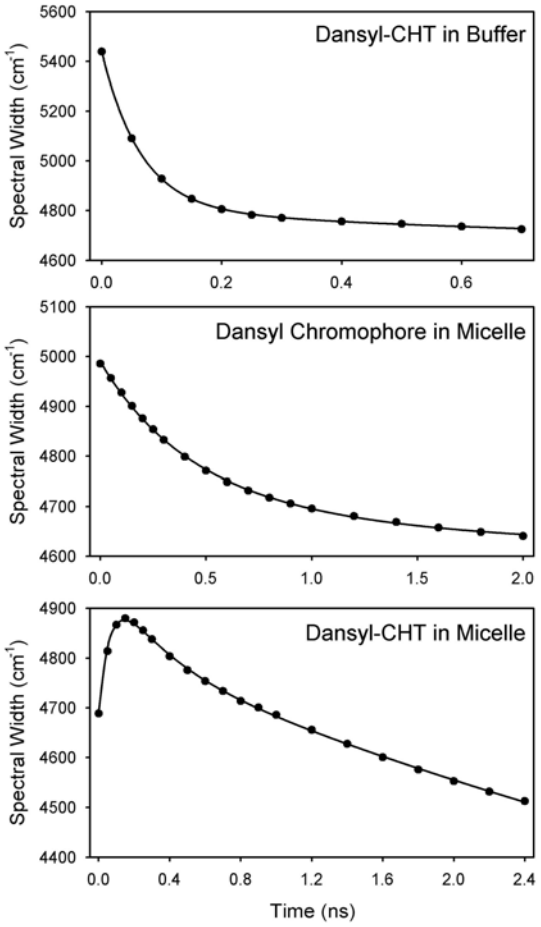

Figure 36. Time-resolved line width (Γ) of TRES of DC at the enzyme surface (*upper*), DC at micellar surface (*middle*) and DC in the CHT-micelle complex (*lower*).

Activity, dynamics and energetics. Upon complexation with the CTAB micelle CHT shows hypo-activity (the study reported here) and superactivity[5] on substrates AMC and PNPA respectively (table 8). The overall retardation and enhancement of the enzymatic activity (k_{cat}/K_m) are estimated to be 7 and 2.5 times respectively. The superactivity[5] of CHT has been correlated with the changes of the secondary structure (e.g. increase in the α-helix content and a decrease in the β-sheet while the turns and unordered contents remained unchanged) compared to the free enzyme in the buffer solution. However, it should be mentioned that the change in the activities in the above studies are *not* sufficient to conclude an important change in the interactions (and/or overall conformations) of micelle-bound CHT with the substrates. For example, if there is a change of stabilization energy of an enzyme-substrate complex by 4 kcal/mol, which is a typical value, associated with a hydrogen bonding interaction at 298 K, the effect on the rate of the enzymatic reaction changes by a factor of 288.

Table 8. Kinetic parameters for the enzymatic activity of CHT with two substrates AMC and PNPA at 27 °C. The parameters for the activity with the substrate PNPA were taken from the work [5]. The free energy for enzyme-substrate complexation is $\Delta G_S = -RT \times \ln(1/K_m)$ [39].

Medium	K_m (μM)	k_{cat} (sec^{-1})	k_{cat}/K_m ($M^{-1}sec^{-1}$)	ΔG_S (kcal mol^{-1})
	Enzymatic hydrolysis of AMC			
Buffer	2500	4.9	1960	-3.55
Micelle	380	0.1	263	-4.66
	Enzymatic hydrolysis of PNPA			
Buffer	44	61.8	1.4×10^6	-5.94
Micelle	29.7	101.4	3.4×10^6	-6.17

The enzymatic activity is shown schematically as follows.

$$\underset{\textbf{\textit{Entrance}}}{E + S \xleftarrow{K_m} E\,S} \xrightarrow[\textbf{\textit{Exit}}]{k_{cat}} E + P$$

Where E, S and P indicate enzyme, substrate and product respectively. The entrance and exit channels of the reaction are also indicated. From table 8, it is evident that CHT-PNPA complex is energetically more stabilized than the CHT-AMC complex in absence of the micelle. As evidenced by relative change of k_{cat} values most significant cause for the retardation of the activity of CHT reported here is the destabilization of the barrier in the exit channel of the micelle-bound enzyme compared to that of the free CHT. The solvation dynamics of the micelle-bound enzyme shows two distinct time constants 150 ps (65%) and 500 ps (35%). The longer one indicates that a significant portion of the enzyme surface (~35%) is in the close vicinity of the micelle to facilitate the interfacial binding with the micelle. In a micellar environment diffusion of the product would expectedly be slower compared to that in free buffer. Slow diffusion from the catalytic site of the micelle-bound CHT and affinity of the product to the micelle that is evidenced by our steady-state anisotropy measurement expectedly *retard* the process of product dissociation from the enzyme resulting destabilization of the energy barrier in the exit channel. Another important observation is a large dynamical Stokes shift in the TRES of the complex (1068 cm^{-1}) compared to that in enzyme in free buffer (74 cm^{-1}), which reveals less amount of missing dynamics within our experimental window. In other words the time constants observed in our experiment are

mostly responsible for the entire relaxation processes at the surface of the micelle-bound enzyme. The observation clearly indicates more rigid environment around the micelle-bound CHT compared to that of free enzyme in buffer. The enzymatic activity of CHT upon complexation with the micelle depends on rigidity of the environment around the enzyme and/or its structural flexibility[37]. The rigid environment in the close vicinity of the enzyme surface may retard the interaction with the substrate resulting the hypo-activity observed in our experiment.

5. Conclusion

There is a wealth of information available concerning the protein encapsulated in the AOT reverse micelle, such as structure of a protein at various water contents, possible location of a protein in the water pool and catalytic behavior of a protein inside the RM. From a number of reports involving different experimental techniques it has been confirmed that structure of CHT in AOT RM with higher hydration degree ($w_0 \geq 10$) remains unperturbed. In our report, we measured the activity of the protein CHT to a substrate AMC in AOT RM and compared them with that in bulk water (aqueous buffer). We found the rates of catalytic reactions in the RM at a constant enzyme concentration are retarded by, at least, two orders of magnitude compared to that in bulk water (buffer). In this way, we examined the effects of the degree of hydration on reactivity of the protein, since the structure were found to be unperturbed for all these RM[16]. Currently, we are examining the effect of degree of hydration at the different sites of the enzyme; e.g. at the surface, site of the catalytic center and also probing environmental information around the substrate included in the RM.

The reported studies on the energy donor C500 selectively excited at the surface of a RM elucidate its solvation dynamics and resonance energy transfer in the RM without and with the enzyme α-chymotrypsin (CHT). The enzyme is known to preserve its native structural integrity in the RM with the degree of hydration ($w_0=10$) used in our experiment[16]. The solvation process of C500 in the CHT-excluded RM was found to be similar to that of the CHT-included RM giving a single exponential decay of the solvation correlation function C(t) with a time constant of ~660 ps. In contrast, the time resolved anisotropy (r(t)) measurement of the donor in the CHT-included RM shows more geometrical restriction on the donor probe C500 compared to that in the RM without CHT. These observations are consistent with the fact that in the CHT-included RM ($w_0=10$) when the diameter of the water pool of the RM is just sufficient to engulf native CHT, the aqueous space (labile type) available to the donor forms an annular shell. The annular aqueous space impose a restriction on the physical motion of the donor C500 as confirmed by r(t) measurement of the

CHT-included RM. However, upon inclusion of CHT in the RM the mobility of the solvent molecules in the close vicinity of the donor remains similar as discussed above. The formation of the annular shell like structure in the CHT included RM is further supported by time resolved spectral line-width analysis of the donor revealing its translational diffusion in the RM without and with the enzyme CHT. From the temporal behavior of the diffusion of the donor in the CHT included RM we estimate the thickness of the annular shell to be ~2.5 Å. The role of this aqueous layer on the structure and functionality of the enzyme CHT included in the RM is extremely important[4,16].

In order to study the change in locations of the hydrophilic acceptor molecules in the RM upon inclusion of CHT and to estimate distances of those acceptors from a donor at the polar surface of the RM, we used steady state and time resolved spectroscopic techniques. The estimated donor-acceptor distances from the steady state fluorescence energy transfer experiments on the CHT-excluded/included RM are in close agreement with those of the picosecond resolved studies except for the acceptor R123. In the case of R123 the estimated donor-acceptor distance measured from the steady state quenching of donor fluorescence in the CHT-included RM was found to be 27.74 Å. However, the time resolved transient of C500 in presence of R123 in the CHT-included RM was found to be similar to that of the donor without the acceptor R123, revealing that the energy transfer mechanism is not of resonance type. It is just re-absorption of the donor emission by the acceptor at a significantly large distance. From these studies it is clearly evident that EtBr and MC540 rearranged their locations near the surface of the RM upon inclusion of CHT. However, the acceptor R123 has to leave the CHT-included RM in order to create a space for the enzyme. It is worth noting that EtBr and R123 both are cationic dyes but behave quite differently when encapsulated in the RM containing CHT. The proper explanation of the incoherent behavior of R123 compared to that of EtBr demands further investigation and is currently the prime focus of our group. These observations may have significance in understanding the enzymatic reactions of RM-bound CHT with hydrophilic substrates. The overall picture, which emerges from our FRET studies RM with and without CHT complex, is depicted in figure 37.

The time resolved anisotropy of the acceptor molecules as shown in figure 22 (table 7) reveals biexponential decays with significantly large residual anisotropy (residual r(t)), which do not decay within our experimental time window. The longer decay components which remain similar for both the RM (CHT-included/excluded) are consistent with those of the donor anisotropies without acceptors, revealing rotational motions of the acceptor molecules as a whole and/or global motion of the RM. The shorter time constants of the r(t) decays could be assigned to the tumbling/segmental motion of the acceptors. Note that indirect excitation of the acceptor molecules (via donor) may have

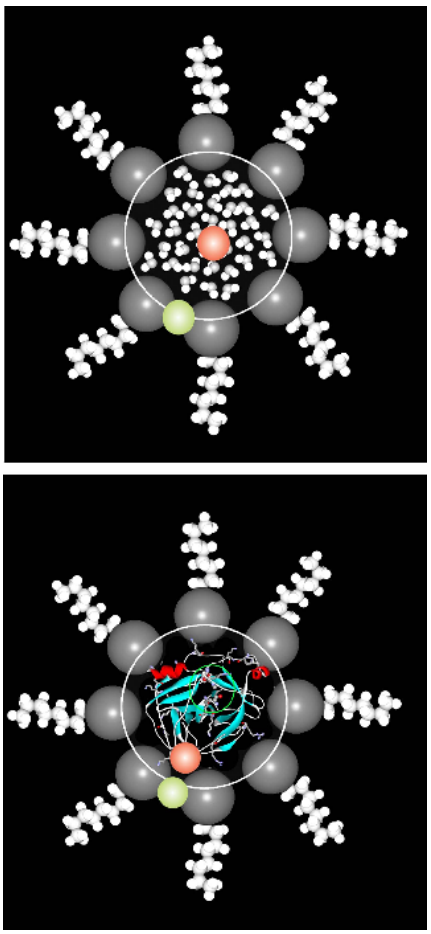

Figure 37. The locations of donor (C500; yellowish green ball) and acceptor molecules (red ball) in the reverse micelle (RM) without (upper) and with (lower) the enzyme CHT are shown schematically. The population of the energy donor C500 at the interface of the RM will only be excited (400 nm excitation). Upper panel indicates that the acceptor molecules reside in the aqueous pool of the RM without CHT. The change in donor acceptor distances upon encapsulation of CHT in the RM is shown in the lower panel. Note the exact numerical values of the donor-acceptor distances in the RM without and with CHT are tabulated in table 2 & 3 (from steady state experiment) and table 5 & 6 (from time resolved measurement).

some effect on the anisotropy values at t=0 (r_0). The time resolved anisotropy of the donor and acceptor molecules revealed significant randomization of the relative orientation of the transition dipoles of the donor and acceptor justifying the value of orientation factor, κ^2, which is assumed to be 2/3 in this study.

Our studies on the DC at the micellar surface demonstrate slow solvation dynamics in the micellar environment (CTAB). The time evolution of TRES shows an exponential decay of time constant 338 ps, which is consistent with other studies of the same micelle using different dye molecule as probe[59].

Picosecond-resolved anisotropy measurement indicates much slower rotational diffusion of the dansyl chromophore in the micelle (1.3 ns) compared to that in bulk solvent (50 ps) [53]. The anisotropy measurement also signifies a possible entanglement of the dynamics of conformational change (twisting; 413 ps) of the probe in the solvation process (338 ps). However, the contribution of the entanglement of twisting in the measured solvation dynamics was found to be insignificant. TRANES analysis of the fluorescence of dansyl chromophore indicates a possible existence of twisted excited CT-state as one of the emissive species.

The dynamical picture of the solvation at the surface of the micelle presented here may have relevance to the function of the micelle in the recognition of the enzyme α-chymotrypsin[5,14]. The labile environment in the close vicinity of the micellar surface would enhance the interaction with the enzyme. On the other hand dynamically rigid environment is needed around the surface to maintain a 3D structure of the micelle. Thus, the timescale of the solvation dynamics is crucial to the tradeoff between the micellar structure and its function of molecular recognition[35], and it is possible that the reported time constant (338 ps) is of fundamental importance for such function.

The overall picture, which emerges from our studies on the CHT-micelle complex, is depicted in figure 38. Solvation dynamics at the surface were measured from the solvent response as probed by the dynamical Stokes shift of the ligand DC during solvation. The solvation process at the surface of CHT in absence of the micelle were found to be mostly ultrafast, less than 50 ps, indicated by very small dynamical Stokes shift with time constant 142 ps. This observation is in agreement with the previous studies of femtosecond resolved hydration dynamics at the protein surfaces[35] and is significant for the recognition of substrate and/or other protein by CHT. The surface of CHT presumably optimize binding of substrate (or other protein/aggregate) involving efficient dehydration process by utilizing labile water, unlike slow structural water layer needed to maintain 3D structure. However, dynamical anisotropy, which probes orientational motions of the ligand DC covalently adducted at the surface of CHT persists for more than 10 ns, in contrast to the behavior at the micellar surface or in bulk methanol indicating restriction of physical motions of the probe DC at the surface of CHT.

The enzyme forms complexes with CTAB micelle[5], which is expected to be sandwich like (figure 38). The steady-state fluorescence also indicates the complexation of DC-bonded CHT with the micelle (figure 24). The solvation process of the complex, which is different from those at the enzyme and micellar surfaces, gives two distinct time constants of 150 ps (65%) and 500 ps (35%) indicating spatial heterogeneity of the local environment of the ligand DC at the interface. The time constant of 150 ps of the C(t) decay is similar to

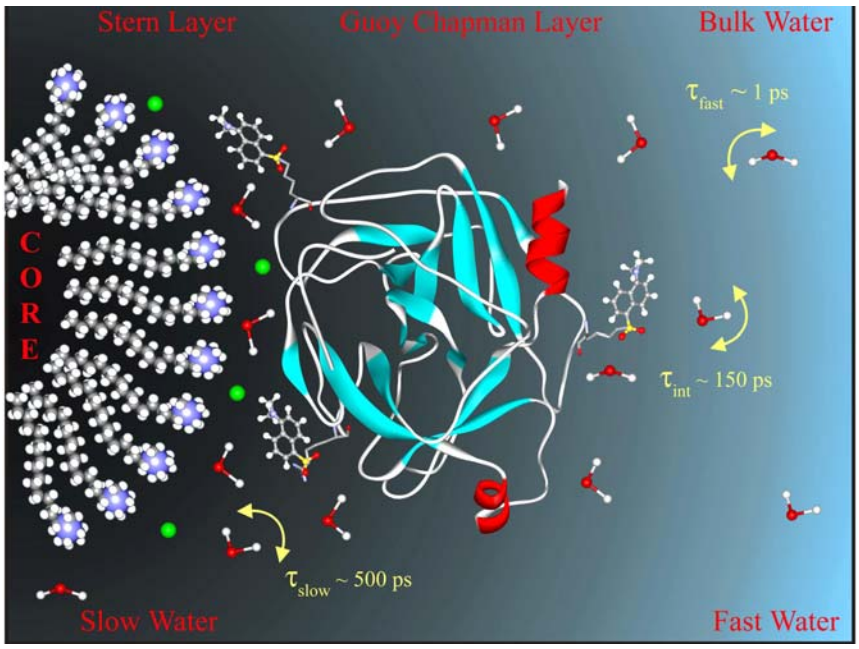

Figure 38. Model of the interaction between the protein CHT and the CTAB micelle, showing interfacial dynamics studied through the covalent labeling of the probe DC (three possible sites were shown using ball & stick model) to the enzyme. The gradient of black color is an indication of variation of hydrophobicity/rigidity of the environments in the CHT-micelle complex. The hydrophobicity decreases gradually from its highest value in the core (black) of the micelle to the lowest one in the bulk water (blue). The distribution of solvation time in the complex defines three types of water motions: Bulk water (weak interaction; ~1 ps), intermediate in the Guoy-Chapman layer (~150 ps) and those much slower (strong interaction; ~500 ps) in the interface of the complex.

the observed slower component of the solvation process at the surface of CHT without micelle. However, it is faster than that at micellar surface (340 ps). As shown in the figure 38, the water molecules in the relatively less rigid environments (Guoy Chapman layer) compared to stern layer of the micelle[65] could also result the faster dynamics. The slower time constant of the CHT-micelle complex (500 ps) is significantly different from those at micellar and enzyme surfaces and can be assigned to be solely due to the interfacial relaxation.

The rigidity of the micelle-enzyme complex was measured by time-resolved anisotropy, which probes orientational motions of the ligand DC covalently adducted at the surface of the enzyme. The dynamical nature of the anisotropy (r(t) decay) is different from those at the enzyme and micellar surfaces, which reveals a structural perturbation as evident from other studies. TRANES analysis of the time-resolved fluorescence spectra of the samples anticipates possible entanglement of emission from the CT state dynamics in

the process of solvation. Studies of picosecond dynamics of the probe DC at the enzyme surface and in the enzyme-micelle interface elucidate nature of biomolecular recognition process and the time scales involved for complex rigidity and solvation. These studies attempt to link structural and dynamical features for insight into the biological function (activity) of the enzyme CHT in restricted (real) environments with controlled degree of hydration.

Acknowledgement

We thank colleagues in our laboratory at S.N. Bose Centre whose contributions, acknowledged in the references, have been instrumental in the successful evolution of work in this area. In particular we thank Ajay Kumar Shaw, Parijat Majumder, S. Shankara Narayanan, Debapriya Banerjee, Anjan Chakraborty and Manoranjan Ghosh. We also acknowledge supports of Drs. Nilmoni Sarkar, IITKGP and Anindya Datta, IITB for time resolved experiments.

References

1. J. A. Rupley and G. Cateri, Adv. Prot. Chem. **41,** 37-172 (1991).
2. M. T. de Gomez-Puyou and A. Gomez-Puyou, Critical Rev. Biochem. Mol. Biol. **33,** 53-89 (1998).
3. A. V. Levashov and N. L. Klyachko, Russian Chem. Bulletin Int. Ed. **50,** 1718-1732 (2001).
4. R. Biswas and S. K. Pal, Chem. Phys. Lett. **387,** 221-226 (2004).
5. M. S. Celej, M. G. D'Adrea, P. T. Campana, G. D. Fidelio, and M. L. Bianconi, Biochem. J. **378,** 1059-1066 (2004).
6. P. Viparelli, F. Alfani, and M. Cantarella, Biochem. J. **344,** 765-773 (1999).
7. N. Spreti, F. Alfani, M. Cantarella, F. D'Amico, R. Germani, and G. Savelli, J. Mol. Catal. B-Enzym. **6,** 99-110 (1999).
8. P. L. Luisi, M. Giomini, M. P. Pileni, and B. H. Robinson, Biochim. Biophys. Acta **947,** 209-246 (1988).
9. M. P. Pileni, Advances in Colloid and Interface Science. **46,** 139-163 (1993).
10. C. M. Carvalho and J. M. Cabral, Biochimie. **82,** 1063-1085 (2000).
11. A. M. Klibanov, TIBS **14,** 141-144 (1989).
12. J. K. A. Kamal, T. Xia, S. K. Pal, L. Zhao, and A. H. Zewail, Chem. Phys. Lett. **387,** 209-215 (2004).
13. P. Majumder, R. Sarkar, A. K. Shaw, A. Chakraborty, and S. K. Pal, J.Colloid and Interface Science **290,** 462-474 (2005).
14. R. Sarkar, M. Ghosh, A. K. Shaw, and S. K. Pal, Journal of Photochemistry and Photobiology B: Biology **79,** 67-78 (2005).
15. R. Sarkar, M. Ghosh, and S. K. Pal, J. Photochem. Photobiol. B: Biol. **78,** 93-98 (2005).
16. A. L. Creagh, J. M. Prausnitz, and H. W. Blanch, Enzyme Microb Technol. **15,** 383-392 (1993).
17. H. H. Paradies, J. Phys. Chem. **84,** 599-607 (1980).

18. S. S. Berr, J. Phys. Chem. **91,** 4760-4765 (1987).
19. S. S. Berr, E. Caponetti, J. S. Johnson, J. R. R. M. Jones, and L. J. Magid, J. Phys. Chem. **90,** 5766-5770 (1986).
20. H. L. Tavernier, F. Laine, and M. D. Fayer, J. Phys. Chem. A **105,** 8944-8957 (2001).
21. X.-G. Lei, G.-H. Zhao, Y.-C. Liu, and N. J. Turro, Langmuir **8,** 475-480 (1992).
22. T. K. De and A. Maitra, Adv. Colloid Interface Sci. **59,** 95-193 (1995).
23. K. Bhattacharyya, Acc. Chem. Res. **36,** 95-101 (2003).
24. M. Hirai, T. Takizawa, S. Yabuki, R. K. Hirai, K. Nakamura, M. Oya, K. Kobayashi, and Y. Ameniya, J.Chem.Soc., Faraday Transactions **91,** 1081-1089 (1995).
25. A. N. Eryomin and D. I. Metelitza, Biochemistry (Moscow) **64,** 1049-1060 (1999).
26. R. P. Haugland, *Handbook of Fluorescent Probes and Research Chemicals*, 7th Ed. ed. (Molecular Probes, Eugene, OR, 1996).
27. L. Michaelis and M. M. L. Menten, Biochemische Zeitschrift **49,** 333 (1913).
28. J. R. Lakowicz, *Principles of fluorescence spectroscopy* (Kluwer Academic/ Plenum, New York, 1999).
29. M. L. Horng, J. A. Gardecki, A. Papazyan, and M. Maroncelli, J. Phys. Chem. **99,** 17311-17337 (1995).
30. A. S. R. Koti, M. M. G. Krishna, and N. Periasamy, J. Phys. Chem. A **105,** 1767-1771 (2001).
31. S. R. Koti and N. Periasamy, Proc. Indian Natn. Sci. Acad. (Chem. Sci.) **113,** 157-163 (2001).
32. N. Periasamy and A. S. R. Koti, Proc. Indian Natn. Sci. Acad. **69A,** 41-48 (2003).
33. D. V. O'Connor and D. Phillips, *Time Correlated Single Photon Counting* (Academic Press, London, 1984).
34. J. J. Birktoft and D. M. Blow, J.Mol.Biol. **68,** 187-240 (1972).
35. S. K. Pal and A. H. Zewail, Chem. Rev. **104,** 2099-2123 (2004).
36. Y. Pocker, Cell. Mol. Life Sci. **57,** 1008-1017 (2000).
37. H. Frauenfelder, P. W. Fenimore, and B. H. McMahon, Biophys. Chem. **98,** 35-48 (2002).
38. S. K. Pal, J. Peon, and A. H. Zewail, Proc. Natl. Acad. Sci. USA **99,** 15297-15302 (2002).
39. A. Fersht, *Enzyme structure and mechanism*, Second ed. (W. H. Freeman and company, New York, 1985).
40. M. Zimmerman, B. Ashe, E. C. Yurewicz, and G. Patel, Anal Biochem. **78,** 47-51 (1977).
41. K. S. Freeman, S. S. Lee, D. J. Kiserow, and L. B. McGown, J. Colloid and Interface Science **207,** 344-348 (1998).
42. E. Ruckenstein and P. Karpe, J. Phys. Chem. **95,** 4869-4882 (1991).
43. C. Petit, P. Brochette, and M. P. Pileni, J. Phys. Chem. **90,** 6517-6521 (1986).
44. V. N. D. Taran, C. Veeger, and A. J. Visser, Eur. J. Biochem. **211,** 47-55 (1993).
45. M. Caselli, P. L. Luisi, M. Maestro, and R. Roselli, J. Phys. Chem. **92,** 3899- 3905 (1988).
46. R. S. Rahaman and T. A. Hatton, J. Phys. Chem. **95,** 1799-1811 (1991).
47. S. D. Bernal, T. J. Lampidis, and I. C. Summerhayes, Science **218,** 1117-1119 (1982).

48. S. K. Pal, D. Mandal, and K. Bhattacharyya, J. Phys. Chem. B **102,** 11017-11023 (1998).
49. D. Mandal, S. K. Pal, D. Sukul, and K. Bhattacharyya, J. Phys. Chem. A **103,** 8156-8159 (1999).
50. P. Dutta, P. Sen, S. Mukherjee, and K. Bhattacharyya, Chem. Phys. Lett. **382,** 426-433 (2003).
51. N. A. Smith, S. R. Meech, I. V. Rubtsov, and K. Yoshihara, Chem. Phys. Lett. **303,** 209-217 (1999).
52. M. Viard, J. Gallay, M. Vincent, and M. Paternostre, Biophys. J. **80,** 347-359 (2001).
53. Zhong, S. K. Pal, and A. H. Zewail, CHEMPHYSCHEM **2,** 219-227 (2001).
54. S. K. Pal, J. Peon, and A. H. Zewail, Proc. Natl. Acad. Sci. USA **99,** 1763-1768 (2002).
55. B. Hartley and V. Massey, Biochim. Biophys. Acta **21,** 58-70 (1956).
56. R. P. Haugland and L. Stryer, in Conformation of Biopolymers (Ramachandran, G. M., ed.; Academic press, New York) **Vol. I,** 321-333 (1967).
57. M. Byler and H. Susi, Biopolymers **25,** 469-487 (1986).
58. B. Ren, F. Gao, Z. Tong, and Y. Yan, Chem. Phys. Lett. **307,** 55-61 (1999).
59. S. K. Pal, D. Sukul, D. Mandal, S. Sen, and K. Bhattacharyya, Chemical Physics Letters **327,** 91-96 (2000).
60. P. P. Mishra, J. Bhatnagar, and A. Datta, Chemical Physics Letters **386,** 158-161 (2004).
61. A. Datta, A. Dube, B. Jain, A. Tiwari, and P. K. Gupta, Photochem. Photobiol. **75,** 488-494 (2002).
62. P. Minton, J. Biol. Chem. **276,** 10577-10580 (2001).
63. S. Verkman, TIBS **27,** 27-33 (2002).
64. O. G. Berg, M. H. Gelb, M. D. Tsai, and M. K. Jain, Chemical Review **101,** 2613-2653 (2001).
65. N. Nandi, K. Bhattacharyya, and B. Bagchi, Chem. Rev. **100,** 2013-2045 (2000).